

Otto-von-Guericke-University Magdeburg  
Faculty of Electrical Engineering and Information Technology  
Chair for Integrated Automation

# Master Thesis



## Machine Learning based differentiation of Human Gait characteristics associated with Normal and Abnormal behaviors using Wearable Sensors

Examiners:  
Prof. Dr.-Ing. Christian Diedrich  
Dr.-Ing. Peter Eichelbaum

Supervisor:  
Dipl.-Ing. Sasanka Potluri

Author :  
Srinivas Ravuri  
Born on December 6, 1993  
Submitted : February 28, 2019

## **Abstract**

Gait is an extraordinary complex function of human body that involves the activation of entire visceral nervous system, making human gait definite to various functional abnormalities. Diagnosis and treatment of such disorders prior to their development can be achieved through integration of modern technologies with state-of-the-art developed methods. This includes methods for determining the characteristic gait events which help in computing spatio-temporal parameters thereby analyzing human gait. Modern machine learning techniques have outperformed and complemented the use of conventional statistical methods in bio-medical systems. However, analyzing a complex function such as human gait depends on specific variables collected from various Sensor sources. In this thesis, we present a wearable sensor system consisting of plantar pressure measurement system and inertial measurement units which provide reliable information to characterize human gait. Furthermore, the data collected from the developed sensor system is visualized in a 3D environment, exhibiting the weight shift during gait phases giving an intuition about the cyclic nature of human gait. We also present a stable and flawless mobile based data acquisition system with an user interface visually guiding the user throughout the experimental process.

The potential of modern machine learning techniques is then demonstrated using artificial neural networks for classification of gait phases. In this thesis we also present the advantage of using genetic algorithm for optimising the parameters of neural networks thereby reducing 80% of parameter tuning time. We exploit the characteristics of normal gait to identify abnormal characteristics associated with various functional gait disorders.

With a stacked LSTM model we propose a methodology to detect human gait abnormalities that are prone to the risk of fall. The computed metrics and gait parameters show contrasting difference between normal and abnormal behaviors and also validate the model output. The proposed approach aims to demonstrate how advanced technologies help in gait diagnosis and treatment systems. At the end, three specific abnormalities involving Spastic, Parkinsonian and Sensory-Ataxic gaits is presented.

**Task of the Thesis in the Original:**

## **Declaration by the candidate**

I hereby declare that this thesis is my own work and effort and that it has not been submitted anywhere for any award. Where other sources of information have been used, they have been marked.

The work has not been presented in the same or a similar form to any other testing authority and has not been made public.

Magdeburg, February 27, 2019

# Contents

<b>1</b>	<b>Introduction</b>	<b>9</b>
1.1	Motivation and Overview . . . . .	9
1.2	Related Work . . . . .	10
1.3	Methodology . . . . .	14
1.4	Scope and Limitations . . . . .	15
<b>2</b>	<b>Fundamentals</b>	<b>17</b>
2.1	Introduction to Gait . . . . .	17
2.1.1	Nature of Gait . . . . .	17
2.1.2	Stance . . . . .	19
2.1.3	Swing . . . . .	21
2.1.4	Gait Parameters . . . . .	21
2.1.5	Normal Gait . . . . .	22
2.1.6	Abnormal Gait . . . . .	25
2.1.7	Summary . . . . .	29
2.2	Inertial Measurement Units . . . . .	29
2.2.1	MEMS Gyroscopes . . . . .	30
2.2.2	MEMS Accelerometers . . . . .	30
2.2.3	Error characteristics . . . . .	31
2.2.4	Complementary filter . . . . .	31
2.2.5	Kalman filter . . . . .	32
2.3	Plantar Pressure Systems . . . . .	32
<b>3</b>	<b>Hardware, Data Logging and Visualization</b>	<b>35</b>
3.1	Hardware System . . . . .	35
3.2	Data Acquisition . . . . .	40
3.3	Data Visualization . . . . .	43
<b>4</b>	<b>Machine Learning based Gait Analysis</b>	<b>45</b>
4.1	Introduction and Motivation . . . . .	45
4.2	Related Work . . . . .	45
4.3	Methodology . . . . .	46
4.3.1	Data collection and Preprocessing . . . . .	46

4.3.2 Data Annotation . . . . .	48
4.3.3 Gait Phase Classification . . . . .	49
4.4 Gait Parameter Estimation . . . . .	54
4.5 Summary . . . . .	54
<b>5 Abnormal Gait Analysis</b>	<b>57</b>
5.1 Introduction . . . . .	57
5.2 Proposed Methodology . . . . .	57
5.3 Network Architecture . . . . .	58
5.3.1 Long - Short Term Memory Networks . . . . .	58
5.4 Experiment and Results . . . . .	61
5.4.1 Experiments . . . . .	61
5.4.2 Results . . . . .	64
5.5 Gait Parameter Estimation . . . . .	64
5.6 Summary . . . . .	66
<b>6 General Conclusions and Outlook</b>	<b>69</b>
6.1 Conclusions on Proposed Frameworks . . . . .	69
6.2 Applications . . . . .	70
6.3 Future Research . . . . .	70
<b>Bibliography</b>	<b>72</b>

## Nomenclature

$a, A$  scalar, also complex valued

$\vec{a}, \vec{A}$  vector, also complex valued

$\times$  vector cross product

$*$  element wise multiplication

$q'$  differential variable

$\hat{y}$  output vector

## **List of Acronyms**

**AI** Artificial Intelligence

**ANN** Artificial Neural Network

**DNN** Deep Neural Network

**EC** End Contact

**GRNN** Gated Recurrent Neural Network

**GRF** Ground Reaction Force

**HMM** Hidden Markov Model

**ISO** International Organization for Standardization

**IMU** Inertial Measurement Unit

**IC** Initial Contact

**LSTM** Long Short Term Memory

**LR** Loading Response

**MLP** Multi-Layer Perceptron

**RMSE** Root Mean Square Error

**SVM** Support Vector Machine

**TS** Terminal Swing

## List of Figures

2.1	Reference planes for Human Gait Analysis [27] . . . . .	18
2.2	Nomenclature of Human Gait [27] . . . . .	19
2.3	Functional gait cycles according to Perry and Burnfield (2010) . . . . .	20
2.4	Pictorial representation of Classical Gait Abnormalities, taken from [31] . .	27
2.5	Coriolis effect to measure angular velocity:Oscillation of the mass m produces another perpendicular oscillation. After calibration, the absolute value of the angular rate can be computed from the oscillation amplitude, while the phase difference between both oscillations yields the direction of rotation [42].	30
2.6	Principle of an accelerometer where the mass m is suspended in such a way that it can oscillate up and down along the axis. When accelerated, the device causes a displacement of the mass with respect to the enclosure [42].	31
2.7	Commercial plantar pressure insole developed by Tekscan [56] . . . . .	33
2.8	Plantar pressure mapping developed by Tekscan [56] . . . . .	34
3.1	Pressure conducting fabric manufactured by Eeontex, works on the principle of piezo-resistive functionality . . . . .	36
3.2	Common sensor structures, conductive copper electrodes are in yellow; polymeric sensor material is in transparent gray: (a) single point sensor structure, (b) single point sensor inter-digital structure, (c) single point sensor fringe electrode structure, and (d) sensor matrix. Sensor matrix structure was designed in this thesis after carrying out several tests regarding homogeneity, repeatability, linearity and hysteresis. . . . .	37
3.3	Insole assembly, with copper electrodes on eva foam substrates and the Eeontex sensing fabric in the center . . . . .	38
3.4	In-sole circuit schematic designed using EasyEDA . . . . .	39
3.5	Printed circuit board mid-assembly showing populated positions of ESP-32 controller, 16-ch Multiplexer, bias resistors (R1 to R5), JTAG connector interface (P1) and LiPo power source connector (H1). Also not shown are positions for the power switch and LiPo batteries . . . . .	39
3.6	In-shoe plantar pressure sensor and the printed circuit board fabricated into an enclosure(left), Sensor setup on the subject (right) . . . . .	40

3.7 User Interface programmed using Java-script, Independent of the device OS version, it is a browser compatible interface can be deployed in any of the modern Android smart phones. Currently running on Android 6.0 (Marsh mellow): (a) First step, user details screen with start button (b) Second step, 20 sec count down timer (c) Third step, Elapsed time screen with stop button . . . . .	41
3.8 DAQ block diagram showing the TCP/IP client - server operations controlled by the user interface. The data is stored into log files in text format. . . . .	42
3.9 Foot anatomical regions, M01 (heel region), M02 (medial mid-foot), M03 (lateral mid-foot), M04 (medial fore-foot), M05 (central fore-foot), M06 (lateral forefoot), M07 (hallux region) and M08 (toes)[115] . . . . .	43
3.10 Visualization of quantitative pressure measured from the custom built pressure sensing insole based on piezo-resistive methodology. The segmented regions are populated with varying color system correlating to the sensor value. . . . .	44
4.1 Walking path; A to D and back to A, A to B (normal speed), B to C (increased speed), C to D (normal speed), D to A (increased speed) . . . . .	47
4.2 Visualization of raw information collected from the sensor system, from top Plantar pressure, thigh orientation and shank orientation in degrees . . . . .	47
4.3 Annotation of input data; valleys as stance phase, peaks as swing phase . . . . .	48
4.4 Preprocessing of segment orientations using Butter-worth 2 <sup>nd</sup> order filter. Also the visualized graph is normalized. . . . .	49
4.5 Architecture of the proposed DNN with 4 deep layers, the input features are the 8 plantar regions, thigh and shank segment orientations, output layer with shape of two classes . . . . .	50
4.6 Genetic algorithm evolution process . . . . .	51
4.7 Model Training Progress (accuracy) . . . . .	52
4.8 Confusion matrix; on classification of stance and swing phases . . . . .	52
4.9 Gait phase classification using Deep neural network . . . . .	53
4.10 Normalized peak pressure values calculated on the dataset acquired from the experiments; a symmetrical distribution of the plantar pressure can be seen in all anatomical regions . . . . .	54
4.11 Stance Ratio (60%); in accordance with definitions of RLA terminology [1]	55
4.12 Step time . . . . .	55
5.1 High-level architecture of the proposed stacked LSTM Network, here N = 30, l = 1 is shown as an example which depicts many to one network model [2]	59

5.2 Components of a standard LSTM cell with weights, biases and activation functions. Input - Output relations are explained below in form of equations. The picture is partially borrowed from . . . . .	60
5.3 Training (blue) and Validation (orange) performance of our proposed stacked LSTM model on normal data . . . . .	60
5.4 LSTM error predictions on healthy gait, shown in this plot are plantar pressure (blue) and predicted error (orange), depicts LSTM was accurate in predictions of normal gait behavior . . . . .	61
5.5 Characteristics of spastic gait [3] and Simulation of the same; LSTM prediction error . . . . .	62
5.6 Characteristics of parkinson gait [3] and Simulation of the same; LSTM prediction error . . . . .	63
5.7 Characteristics of sensory ataxic gait [3] and Simulation of the same; LSTM prediction error . . . . .	65
5.8 LSTM error predictions on simulated gait abnormalities, shown in this graphic are error plots from top to bottom: Normal, Spastic, Parkinson and Sensory-ataxic gaits. This predicted error is used as a detection metric of abnormality . . . . .	66
5.9 Comparison of Gait parameters; NPP and Stance Ratio . . . . .	67
5.10 Comparison of Step time between normal gait and simulated abnormal gaits	68

## **List of Tables**

1.1	Gait phases, initial contact(IC); loading response(LR); mid stance(MS);terminal stance(TS);pre-swing(PS);end contact(EC); swing(SW) . . . . .	11
1.2	Spatio-temporal parameters . . . . .	13
2.1	Overview of gait parameters subjective to their respective applications . . .	22
2.2	Prevalence of Neurological Gait Disorders in 117 Community-Dwelling Adults [31]. . . . .	26
3.1	Characteristics of Eeontex Pressure conducting fabric . . . . .	37
5.1	Comparison of gait parameters between Normal and Abnormal behaviors .	66

# **1 Introduction**

## **1.1 Motivation and Overview**

The field of Bio-medical engineering endeavors to improve health care by the development of technical methodologies which are used for enhancing the process of diagnosis and treatment of physiological diseases and disorders. Fundamental ways in which diagnosis systems can be improved is by incorporating new technologies and by novel systems and algorithms that make most of these technologies. One of the recent developments in technology is the affected reduction of cost and form factor in micro-electro-mechanical-systems. Due to this, development, Wearable sensor systems have fostered a dramatic growth which opened possibilities of numerous applications, ranging from clinical, sport and recognition systems. Constant research and development in the use of this technology shows that wearable systems have become a part of standard clinical evaluations. This helps the general physicians to understand and improve systems involving high intricacy and complex dynamics.

The interest for wearable systems arises from the need for monitoring individuals on a long-time basis when a physician desires to analyze the situation of the diagnosed acute events, where the chronic condition of the individual includes a risk. Wearable systems are completely non-obtrusive devices that allow physicians to overcome the limitations of other technologies and complete the monitoring process over weeks and if desired over several months. The sensors in this technology are generally fabricated into miniature modules than can be worn inside such as a shirt or a shoe. The data recorded using these systems is processed by algorithms to predict events of possible risks of the individual's clinical status or the data can also be used to explore the impact of clinical interventions.

The goal of this thesis is to use wearable technology through integrating sensors such as IMUs, In-shoe plantar pressure measurement systems with adaptive Artificial Intelligence (AI) algorithms to identify significant events in human gait. Detection of such events help us to identify the abnormal characteristics that occur in an irregular timely fashion. Such algorithms also allow us to verify the reliability of sensors in clinical evaluation. Besides these the thesis also explains the fundamentals of human gait and an equally significant goal; is to describe how advanced solutions for diagnosis of Abnormal gait behavior can be developed by employing artificial neural networks.

## 1.2 Related Work

A systematic literature research was carried out to find related works to the goal proposed here. The publications researched were mostly focused on wearable sensor systems used for human gait analysis. Studies evaluating kinematic gait parameters such as joint angles, gait phases, spatiotemporal parameters of normal and abnormal subjects were only included if they used artificial intelligence algorithms for processing the data. The examined papers are divided into groups according to their topics (i) joint angles [4–6], (ii) gait phases [7–17], (iii) spatiotemporal parameters [8, 18–22] (iv) other approaches: use of machine learning algorithms to differentiate groups based on their gait characteristics (normal or abnormal) [23, 24]

(i) Joint Angles: Different joint angles were estimated by Chalmers et al., Goulermas et al. and Findlow et al. [4–6]. Chalmers et al. measured ankle angle, using a triaxial accelerometer sensor placed on the dorsal part of single shoe. They achieved an RMS error of  $4.9^\circ$  in normal walking and  $6.5^\circ$  in an abnormal walk containing toe walking with fuzzy c-means clustering. Goulermas et al. and Findlow et al. focused on ankle, knee and hip angles with IMUs positioned on the leg segments, foot and shank. Using a general regression neural network (GRNN), both studies achieved high intra-subject predictions, but lower inter-subject predictions compared to other measurement systems. AI algorithms are seldom used to evaluate joint angles. Three studies were found, but two of them [5, 6] belong to one research group. Their algorithm showed a good possibility of measuring joint angles even for inter-subject predictions [23, 24].

(ii) Gait Events: Appropriate classification of gait events as well as the latency was detailed in different research studies. Especially for real-time applications, the detection delay is a significant factor. Some research studies showed the classification of most common gait events, initial contact and end contact [9, 12, 13, 15, 16], some focused on additional events [7, 8, 11, 14, 20, 22]

Yuwono et al. [23] used a wearable IMU sensor and a Bayesian filter to evaluate Initial Contact (IC). They showed, that the IC could be detected using only gyroscopic data with an accuracy of about 90% while using additional acceleration information increased the detection accuracy of about more than 97%. Mijailović et al. [15] used an Artificial Neural Network model to determine IC and End Contact (EC) using six accelerometer sensors positioned along the legs. The relative error was 11% for intrasubject and 14% for inter-subject estimation. Using a Gaussian model, Aung et al. [13] detected IC and EC during inclining and declining gait and also by walking on different terrains with accelerometers employed on feet and ankles. The detection accuracy for all conditions was

more than 90%. On foot accelerometers showed a slightly better performance in terms of accuracy.

Accelerometers placed near to the vertebra (pelvis), González et al. [12] assessed detection of IC and EC in real-time. The algorithm developed by them was able to spot all gait events with an average delay of 117 ms for the initial contact, 34 ms for the end contact. Bejarano et al. [9] developed a real-time machine algorithm on healthy subjects at three different walking speeds, varying walking speeds, and on stroke subjects with IMU sensors positioned at the individuals' shank segments. All ICs and ECs were detected in healthy walking, for patients with severe disabilities it was decreased to 99.3% for IC and 87% for EC. The delay increased from 13.66 ms to up to 52.37 ms.

Williamson and Anderson [8] employed a uniaxial accelerometer placed on the shank segment to determine various gait events Table 1.1 with the help of two different supervised machine learning algorithms. The detection of Terminal Stance was to be most difficult while Loading Response and Swing showed the best results. Rueterbories et al. [7] examined different gait events Table 1.1 in healthy and hemiplegic subjects with sensors placed on the foot using a state machine algorithm . A high accuracy could be shown for the healthy subjects while the detection accuracy for the hemiplegic subjects was heavily reduced. Additionally, the detection delay increased for the hemiparetic subjects.

Authors	IC	LR	MS	TS	PS	EC	SW
Aung et al. [13]	x					x	
Bejarano et al. [9]	x					x	
González et al. [12]	x					x	
Mijailović et al [15]	x					x	
Guenterberg et al. [17]	x		x			x	x
Mannini et al. [14]	x		x	x	x	x	x
Taborri et al. [11]	x	x		x		x	
Williamson et al. [8]		x	x	x	x		x

Table 1.1: Gait phases, initial contact(IC); loading response(LR); mid stance(MS);terminal stance(TS);pre-swing(PS);end contact(EC); swing(SW)

Mannini et al. [10] developed a real-time algorithm a hidden Markov model (HMM) to detect gait events using gyroscopes mounted on foot. The authors showed a detection accuracy of 100% and delay of less than 43 ms for real time applications. For IC and EC the delay was further reduced. Earlier, Mannini and Sabatini [14] achieved slightly inferior results using another HMM. Guenterberg et al. [17] used HMM to classify gait events with the help of eight IMU sensors placed on the limb segments such as forearm, thigh and ankle to examine the sensor position and type to account for the highest possible accuracy. Their results showed that thigh sensor along with all other sensors lead to the

best result. They concluded their work by signifying the importance of the thigh sensor. Taborri et al. [11] also used a real-time algorithm based on HMM to process data from on foot triaxial gyroscopes, shanks and thighs to investigate the best sensor position. They concluded by showing on the best results obtained when using a single on foot sensor. Using more than one sensor the accuracy could be improved. The mean detection delay for all gait events was 60 ms.

Sensor type and position varied between different research groups. Some groups used single accelerometer sensor [7, 8, 12, 13, 15] or gyroscopes [10, 11, 14] other groups used IMU sensors consisting of accelerometers, gyroscopes and magnetometers [9, 16, 17]. The choice of sensor neither showed an association to the parameters evaluated nor to the application of the system. The detection accuracy for IMU and gyroscope-based algorithms were higher than for algorithms based on accelerometers alone. Most commonly, sensors were placed on the lower limb extremities. Taborri et al. [11] found the best placement for a gyroscope only to be on the foot while Bejarano et al. [9] reached the same accuracy with an IMU placed on the shank. Although there is no standards for sensor placement, the most commonly used sensor positions, independent of the type of sensor used, are foot and shank leading to the highest detection accuracy and the low latency. Guenterberg et al. [17] also achieved an accuracy of 100% using an IMU positioned on the thigh segment, but Mijailović et al. [15], who placed three accelerometers along the lower limbs, only achieved an accuracy of less than 90%. Both studies did not specify the detection delay.

In-shoe plantar pressure measurement systems are another subset of Wearable technology. Unlike inertial sensors which have axes components, plantar pressure sensors don't account for the components of the force measures on all axes. Wearable in-shoe sensors are flexible, portable and allow data collection in various terrains. In 2011, a paper describes about a dynamic plantar pressure platform for human identification using a Flex Force in-sole pressure sensor [25]. Cunguang Lou [26] developed a flexible pressure sensor based on the piezo-resistive effect of multilayer graphene films which was used to classify gait phases. Commercially available sensor systems such as sensors from Vista medical, Novel and Tekscan have also shown promising results, which is the main reason where these systems are being employed by most of the physicians. I-Ju Ho1 [27] divided the foot into eight different regions and examined the significance of each region in the classification of gait phases.

### (iii) Spatiotemporal parameters

Besides classifying the gait phases, Mannini et al. [10] related over-ground and treadmill walking. Although they were not able to produce reference data, the tendency for the assessed parameters 1.2 shows no difference among them. Additionally [22], used the

methodology to associate the performance of two different algorithms for determining gait velocity and walking distance in normal people and abnormal people (stroke patients) using IMU sensors mounted on foot, with variation in walking speeds the proposed algorithms' accuracy was between 91% and 96%. Dobkin et al. [19] assessed the outdoor walking speed also of post-stroke patients using only accelerometer positioned on the shank. The correlation Coefficient was 0.98 ( $p = 0.001$ ). Mannini and Sabatini [22] and Dobkin et al. [19], achieved highest prediction accuracies and correlations compared to other measurement systems though they used varied sensor types and locations.

Authors	Stride time	Step time	Stance time	Gait velocity	Cadence
[19]	x	x	x	x	x
[21]	x	x	x		x
[14]	x		x		x
[16]					x

Table 1.2: Spatio-temporal parameters

Yuwono et al. [16] computed cadence and stride symmetry from the IC, from which they determined to get additional information about temporal parameters.

López-Nava et al. [21] measured temporal gait parameters of young individuals and older healthy adults with an accelerometer placed on the ankle. Using a Bayesian model, they were able to determine the parameters displayed in 1.2, as well as IC, EC, number of strides, number of steps and swing time. IC, EC and the number of steps and strides were predicted with 100% accuracy. Stance and swing phase time the relative estimation error was higher than 5%. Compared to a standard system (GaitRite), the weakest correlation was found for the swing phase time with 74%. Additionally, they classified single support and double support time. Samà et al. [20] estimated step length and gait velocity from a single waist worn IMU sensor. Santhiranayagam et al. [18] estimated, minimum toe clearance of healthy young and older subjects using an IMU sensor mounted on foot. This gait parameter describes the minimum height of the toe during mid swing and is used as a predictor for fall risks. Using a GRNN they achieved an Root Mean Square Error of 7 mm, which was within one standard deviation of the group mean.

#### (iv) Other Approaches

Mannini et al. [23] used HMM and a supervised machine learning method SVM to classify different pathological gaits using sensor data from IMUs positioned on the shank. Therefore, they detected IC and EC from stroke patients, Huntington's disease patients and healthy subjects. They achieved an overall classification accuracy of 90.5%. All misclassification occurred between the two different impaired populations. Zhang et al. [28] used SVM

to classify fatigue and non-fatigue gait of healthy subjects. The IMUs were placed at the right shank and the sternum. The estimated parameters were step length and width, heel contact velocity and single stance time. The intra-subject classification accuracy was 97%, the inter-subject classification accuracy was 90%. Yang et al. [29] clustered complex regional pain syndrome patients and healthy subjects into groups. They explored amongst others the parameters step time and cadence with an accelerometer placed at the lower back. Comparative analysis of supervised machine learning methods showed classification accuracy up to 99.38%.

J. Hannink et al. [30] used an ensemble approach to outperform most of the methods in the research for calculating gait parameters. Foot mounted IMU sensor data was used in conjunction with deep learning on a clinically relevant and publicly available benchmark dataset briefly described here <https://www5.cs.fau.de/activitynet/benchmark-datasets/digital-biobank/> and , they were able to estimate stride length, width and medio-lateral change in foot angle up to  $0.15 \pm 6.09\text{cm}$ ,  $0.09 \pm 4.22\text{ cm}$  and  $0.13 \pm 3.78^\circ$ respectively. Stride, swing and stance time as well as heel and toe contact times are estimated up to  $\pm 0.07$ ,  $\pm 0.05$ ,  $\pm 0.07$ ,  $\pm 0.07$  and  $\pm 0.12\text{ s}$  respectively

Tanmay T. Verlekar [31], developed an automatic system to classify gait impairments using a marker less 2-D video-based information. The system relies on two different types of features to perform classification: (i) features such as step length, step length symmetry, fraction of foot flat during stance phase, normalized step count, speed; and (ii) body-related features, such as the amount of movement while walking, center of gravity shifts and torso orientation. SVM was used as a classifier and results show that the proposed system outperforms existing marker-less 2D video-based systems, with a classification accuracy of 98.8%.

A vision-based system to classify normal and abnormal gait features was developed by Mario Nieto-Hidalgo [32], analyzing image frames to identify gait features to determine the spatiotemporal parameters (heel strike, toe off, stride length and time) and skeleton joints they present a system with an algorithm capable of automatically extracting kinematic features characterizing human gait as normal or abnormal.

### 1.3 Methodology

An in-depth review of relevant literature's was performed at the initial phase of the thesis which gave us a clear insight and a deep understanding of our research goal. Overcoming the challenges and limitations in terms of the sensor placement and accuracy faced by the researchers was also strongly considered.

The present thesis is focused on contributing to the constant improvement of gait assessment systems in the context of wearable technology. The system was developed with the primary goal of differentiating the gait features associated with Normal and Abnormal gait characteristics. Therefore, such systems could be applied in various fields ranging from sport, clinical and recognition systems. Chapter-2 provides a clear insight into the fundamentals of gait and the characteristics associated with Normal and Abnormal gait behaviors. It also explains about the current state of the art wearable sensor technology. Chapter-3 showcases the sensor system hardware and software that was designed and developed suitable for the current goal. The limitations of using conventional methods for detecting normal and abnormal gait characteristics are also outlined. In Chapter-4 the methodology of gait analysis associated with normal gait using wearable sensor technology is extended with the use of AI algorithms with a primary objective on improving the accuracy, applicability, robustness and reliability of the sensor system. Machine Learning algorithms (supervised) used in this context have shown accurate and robust outputs which make them as an obvious choice, as they become more useful for bio-medical applications.

The most important goal of this thesis was to demonstrate how such advanced algorithms can be used in assisting diagnosis systems for detecting gait disorders. Such systems can be developed through integrating the wearable sensor technology with advanced machine learning algorithms. Chapter-5 explains and also demonstrates an automatic abnormality detection using a recurrent neural network trained on normal kinematic features. A threshold of divergence or deviation predicted by the algorithm was defined as a relative error. The resulting prediction errors are modeled as a multivariate Gaussian model, which is used to evaluate the possibility of abnormal behavior. Subsequently, a comparative analysis showing the difference of parameters between normal and abnormal gait is presented. Both systems are evaluated in experiments that demonstrate the advancements one can achieve with respect to the current state of the art by combining modern technologies. Chapter-6 concludes with applications discussed in-detail where the developed sensor system can be used for predicting such abnormalities in gait.

## **1.4 Scope and Limitations**

The scope of this project is mainly focused on detecting the gait characteristics associated with any kind of abnormal behavior. Three specific abnormalities are discussed in the later sections and factors such as applicability and reliability of the system are also presented. Significant points that make this thesis stand out from existing state-of -the art techniques are: (i) Determining the incidence of gait disorder prior to its occurrence provided a substantial amount of available data from the respective individual. (ii) A visual

representation of the model error predictions. (iii) The scope of the developed hardware system could also be extended and customized for specific applications in the context of assisting functions for diagnosis and treatment applications in bio-medical industry. A possibility is provided for embedding external modules such as IMU's, temperature sensors and pedometers into the plantar pressure insole system which can also be considered as another area of research and development.

Determining the type of abnormality is completely out of scope for this project. Due to unavailability of the subjects intra-subject analysis was not performed as it required the data from equivalent individuals over a long period of time. The analysis presented only refers to inter subject predictions.

## 2 Fundamentals

In this chapter let us review the fundamentals in order to develop a comprehensive understanding of the concepts that are discussed in the following chapters. In Section 2.1, the fundamental concepts of gait and its cyclic nature are defined. In Section 2.2 a brief overview about working principle of IMU's, error characteristics and algorithms commonly used to compensate such errors are presented. A brief review about In-shoe Plantar pressure measurement systems is then presented.

### 2.1 Introduction to Gait

Gait can be outlined as a certain way of motion, achieved on foot like walking or running, or in short gait is a manner of walking unique to each being. The scientific description of walking and artificially simulating it in a robot is much more intricate than the act of walking itself. Although no robot or orthosis has been built, that realizes a quality of walking comparable to that of the human gait in terms of its efficiency and stability. The analysis and modeling of human gait and design of orthosis and exoskeleton have yielded productive intuitions about the nature of gait.

#### 2.1.1 Nature of Gait

The human body has three primary planes which include sagittal, frontal and transverse. But in most studies the main emphasis is given to the sagittal plane see figure 2.1, overlooking the three dimensional nature of human gait [33]. Any gait is considered functional based on the two main requisites

- Periodic motion of each foot from one spot to next to support the body
- Adequate ground reaction forces applied at the foot contact

These two fundamentals are essential for bipedal gait, even in case of distorted patterns observed in pathology. And the periodic motion of the feet observed during gait is the essence of its cyclic nature. To understand the periodicity of gait better, the gait phases

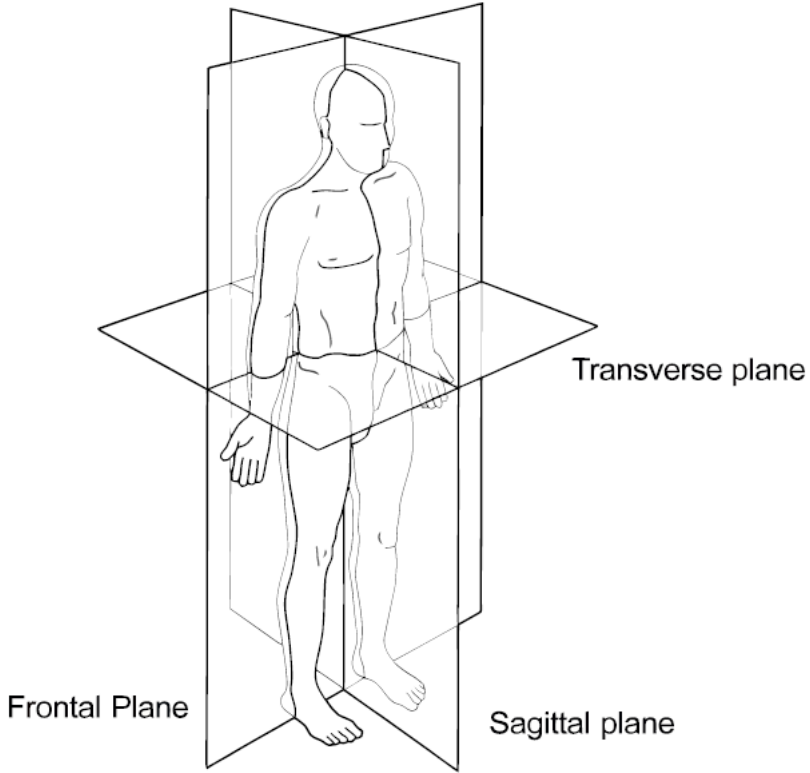


Figure 2.1: Reference planes for Human Gait Analysis [27]

must be used to describe the entire gait period. To reduce ambiguities in gait phase nomenclature, the Rancho Los Amigos (RLA) gait analysis committee established a generic terminology for the functional phases of gait [1]. RLA terminology is currently preferred, because it describes gait more in terms of processes or temporal fragments, and it is semantically more generic. The gait data was classified based on the terminology defined by RLA gait analysis committee. As per [34], a healthy gait cycle is split into eight distinct gait phases -initial contact, loading response, mid-stance, terminal stance, pre-swing, initial swing, mid swing, and terminal swing (see Figure 2.3). While traditional nomenclature of the gait phases is represented in Figure 2.2. The gait cycle is characterized into two main phases,

- Stance
- Swing

One complete gait cycle comprises of both a stance and swing phase. During stance phase, the foot is in contact with the ground and equates to 60% of the gait cycle. Whereas in swing phase that same foot is no more in contact with the ground and the leg is swinging over in preparation for the following foot strike. The swing phase makes up the remaining

40% of the gait cycle (see Figure 2.2). As seen in Figure 2.3, the stance phase may be subdivided into three separate phases:

- First double support - here both the feet are in contact with the ground.
- Single limb support - occurs when the right foot is in ground contact and the left foot is swinging through.
- Second double support - double support occurs for the second time when both feet come into ground contact at the end of the gait cycle.

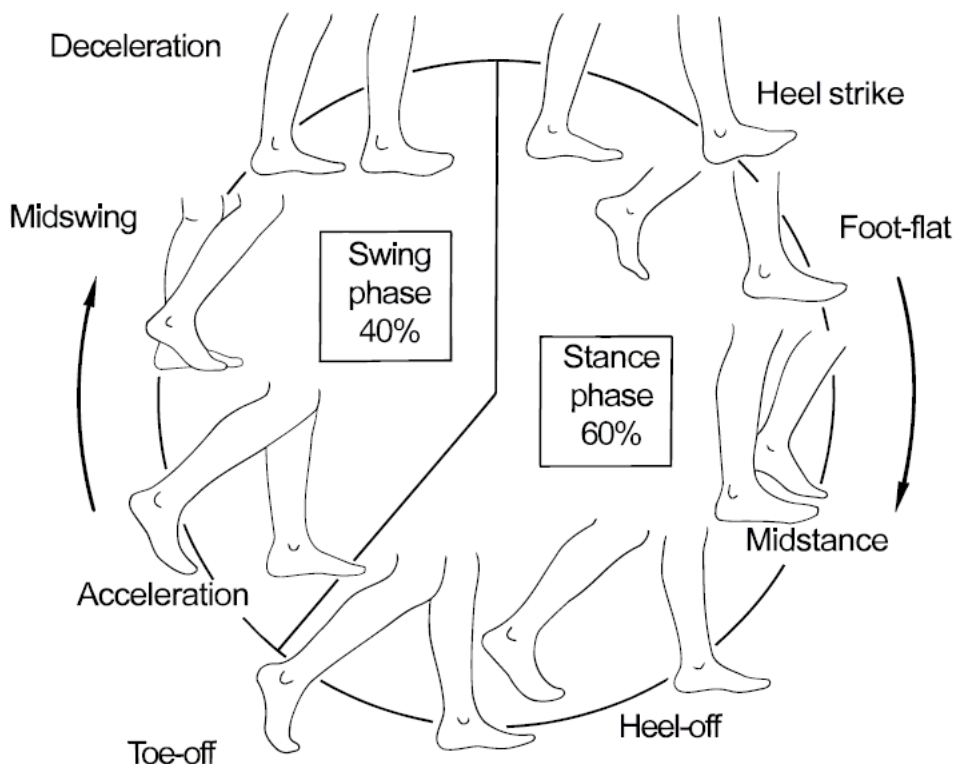


Figure 2.2: Nomenclature of Human Gait [27]

### 2.1.2 Stance

- *Initial Contact (Heel strike)* - This phase comprises of the instant when the heel touches the floor. The joints posture of this phase initiates the gait cycle, and also indicates the point at which the body's center of gravity is at its lowest position. IC is truly an instant in time, rather than a phase. This event is important to take note of because it determines the limb's loading response pattern and is the beginning of double limb support.
- *Loading Response (Foot flat)* - The point where the plantar surface of the foot comes

into contact with the ground. The phase begins with IC and proceeds until the other foot is lifted for swing. With the heel functioning as a rocker, and the knee being flexed aiding rapid weight transfer, the shock created on the outstretched limb is swiftly absorbed. This phase covers the entire first double support period and in the interval of 0 – 10% of the gait cycle.

- *Mid stance*- Mid stance occurs when swinging foot passes the stance foot and shifting the weight from the rear, to the front using the built up momentum. Here the body's center of gravity is at its peak position. This phase is the first half of the single-limb support interval and covers 10 – 30% of the gait cycle. The movement is facilitated by the ankle dorsiflexion (ankle rocker), while the knee and hip extend.

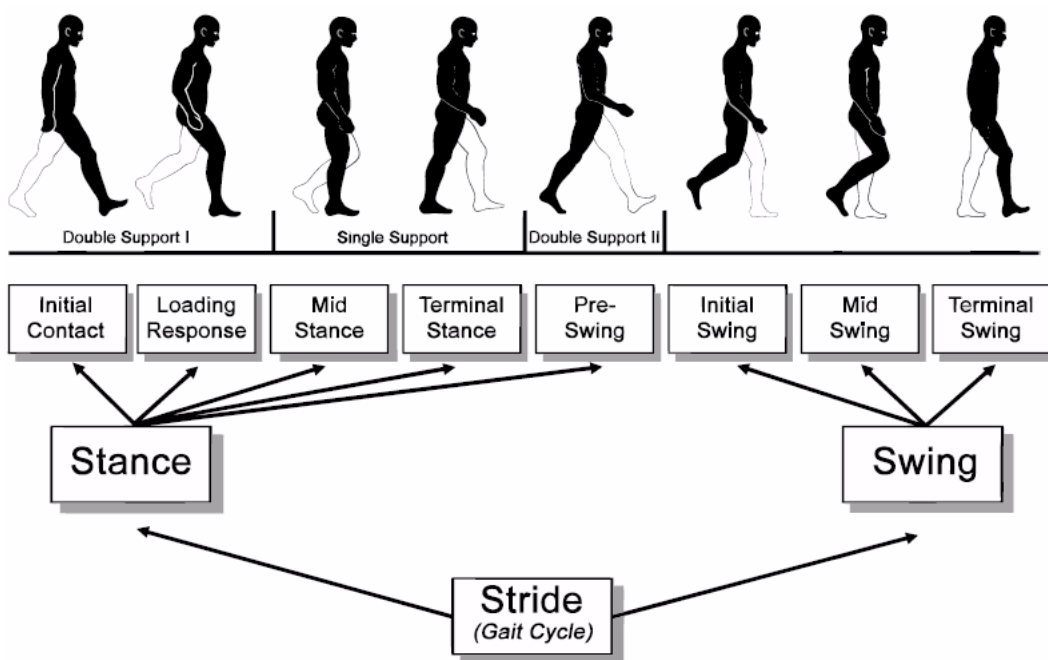


Figure 2.3: Functional gait cycles according to Perry and Burnfield (2010)

- *Terminal Stance* - This phase concludes the period of single-limb support and covers about 30 – 50% of the gait cycle. The stance starts with the heel going up and lasts until the other foot strikes the ground, with the limb advancing forward. During this phase, the body weight advances ahead of the forefoot.
- *Pre-swing* - This is the final phase of stance and is part of the second double support interval. This phase covers about 50 – 60% of the gait cycle. Pre-swing commences with the initial contact of the other limb and finishes with the ipsilateral toe-off. The objective of this phase is to situate the limb for swing. This phase is also termed as “weight release” or “weight transfer”.

### 2.1.3 Swing

- *Initial Swing (Acceleration)*-The acceleration begins immediately after the foot leaves the ground and the activation of the hip flexor muscles to accelerate the limb forward culminating when the swinging foot is opposite the stance foot with maximum knee flexion. This phase is approximately one-third of the swing period and about 60 – 73% of the gait interval. In this phase, the foot is raised, and the limb is progressed by hip flexion and greater knee flexion.
- *Mid-swing* - The phase occurs from the instant of maximum knee flexion and the forward movement of the tibia to a vertical position (hip and knee flexion postures are equal) covering 73 – 87% of the gait cycle. The knee is permissible to extend in response to gravity, while the ankle continues dorsi-flexion to neutral. Limb advancement and foot clearance are the two important objectives of this phase.
- *Terminal Swing (Deceleration)* – This phase describes the action of the muscles as they slow the leg and stabilize the foot in preparation for the next heel strike. This final phase of swing concludes when the foot strikes the floor covering 87-100% of the gait cycle.

There is a functional objective for each gait phase and every phase is part of a critical synergistic motion of a successful or healthy gait. While a motion that is not symmetric in nature is termed as unhealthy or abnormal gait. The sequenced coordination of the gait phases allows the limb to achieve three tasks; the tasks of weight reception, single-limb support, and limb progression. Weight reception starts the stance part of gait with initial contact (heel-strike) and loading response (foot-flat). The stance continues as single-limb support by the mid-stance and terminal stance. While, limb progression starts with pre-swing and extends through initial, mid, and terminal swing. The analysis of the gait phases and knowledge of the fundamental tasks of limb movement, prove that the gait phase detection can be effectively accomplished from accurate orientation data of the leg segments.

### 2.1.4 Gait Parameters

The complex dynamical nature of human gait is not entirely clear and understanding this behavior has become a topic of major research interest. Qualitative and quantitative assessment of gait is usually performed by considering various parameters that describe human gait. Such parameters help physicians to understand the bio-mechanics involved in human gait and also help in clinical diagnosis. Depending on the field of research, the

parameters of interest of human gait vary (see Table 2.1).

Gait Parameter	Clinical applications	Sport applications	Recognition
Stride Velocity	x	x	x
Step length	x	x	x
Stride length	x	x	x
Cadence	x	x	x
Step width	x	x	x
Step angle	x	x	x
Step time	x		
Swing time	x		
Stance time	x		
Traversed distance	x	x	
Gait Autonomy	x		
Stop duration	x		
Tremors	x		
Fall	x		
Accumulated altitude	x	x	
Route	x	x	
Gait phases	x	x	x
Body segment orientations	x	x	
GRF's	x	x	
Joint Angles	x	x	
Muscle force	x	x	
Momentum	x	x	
Body posture	x	x	x
Long-term monitoring of gait	x	x	

Table 2.1: Overview of gait parameters subjective to their respective applications

Researchers have standardized several of these parameters of gait as shown in the table and also have recognized clearly their relations with different medical pathologies. Almost a decade back, the sensor platforms available were not reliable and accurate to quantify gait parameters in a realistic situation (e.g. during sport activities or during walking in a natural terrain etc.), so as to assess the state of health of a person's gait. Then wearable sensor systems were introduced recently to cope with this.

### 2.1.5 Normal Gait

Normal Gait is determined by its rhythmic nature where the lower extremities move in an alternating propulsive fashion.

## Ankle/Foot

Although the orientation ranges of ankle are quite small, they are vital for shock absorption and for the forward motion of the body's center of mass. The flexing of the ankle plantar occurs during the time of loading response. The single support initiates dorsiflexion while advancing the rotating tibia over the fixed foot. At the end of the double support, maximum flexion is attained around 30 degrees at toe-off.

This further initiates the swing phases with dorsiflexion. The ankle's motor control is well understood as the muscle activity in the swing phase commences. At the pre-swing phase the dorsiflexors of the ankles experience short eccentric contractions, continued immediately by concentric contractions at the start of initial swing. This sequence of muscle contractions enhances efficiency and guarantees foot clearance. This neutral or somewhat dorsiflexed pose is maintained throughout the swing phase by the isometric contraction of the pretibial muscle. Following loading response is signified by control of plantar flexion by the pretibial muscles with eccentric contractions. Also, at the ankle plantar dorsiflexors and flexors a short time co-contraction occurs to increase limb stability. This co-contraction helps to smooth the transition between initial double support and single support.

The coupling of the dorsiflexion in loading response with eversion (i.e. sole turning away from the median plane) occurs due to the ankle orientation and subtalar axes. These two actions are smoothed out by the eccentric contractions of the posterior tibialis. The ankle plantar flexors start to generate force during single support, reaching maximum force between terminal stance and pre-swing. The shock absorption possible during the single support is due to the fact that the forward tibial rotation is restrained. The ankle plantar attains maximum flexing during pre-swing due to the triceps-surae muscle groups (calf muscle).

But the role of triceps-surae in pre-swing is debatable. As other research which describes preswing as push-off suggests that, the propelling of the limb is carried out by the ipsilateral calf. Another model by Perry, denounces the contribution of the ipsilateral calf muscle. An alternative model presents an opposing fact to the ankle plantar flexion propelling the body forward. It proposes that the ankle plantar flexion initiates the flexion at the knee and the hip region as a preparation for swing. This could be well observed in transtibial amputees (individuals with poor plantar flex), who normally require greater assistance of power in the knee and the hip region during pre-swing.

## Knee

Majority of the knee motion is restricted to the sagittal plane. The total motion of the knee starts from knee flexion of about 5 degrees at initial contact to almost 20 degrees of flexion at the termination of loading response. This is continued by knee extension during single support, with maximum extension occurring at 40% of the gait cycle, during stance phase. The knee flexes rapidly at the transition of terminal stance to pre-swing, enduring till knee flexion angle of 60 degrees through initial swing. As this continues to terminal swing the knee flexion changes to knee extension. Slightly before the termination of the swing phase is the point of maximum knee extension, and is continued by minor flexion as a preparation for the succeeding stance phase.

The function of knee muscles is well understood by beginning the analysis from swing phase. The knee flexion is passive at the onset of the swing phase, due to the active state of hip flexion and the plantar flexion. During swing phase, the hip transits from flexion to extension due to change in the direction of hip joint, which also passively extends the knee. The knee extensions start decelerating from mid-swing due to the action of the hamstring muscles, while the quadriceps muscle becomes active during terminal swing and continues to be so till loading support. These flexions and extensions of the knee help prepare the limb for following weight acceptance. These eccentric muscle actions smoothens the shock that is created during weight acceptance, while limiting the knee flexion (< 20 degrees). In the mid-stance phase during the passive extension of the knee, both the quadriceps and the hamstring muscles are dormant.

## Hip

The hip muscle named gluteus maximus hold primary control over the hip region. This muscle's relative intensity and timing are comparable to that of the hip extensors like the hamstrings. This gluteus maximus works to reverse flexion in the hip region to extension during terminal swing. The gluteus maximus being the strongest muscle group controls the hip from excessive flexing that may occur due to presence of external forces during loading response. The adductor magnus muscle group also demonstrates a similar role and profile. Hence the hip region demonstrates extensive frontal plane motion compared to the knee and ankle. When the body is in single support, the total mass of the body tends to rotate around the hip joint axis of the stance limb. The transition of the stance phase to swing phase is characterized by hip flexion where the trailing limb advances to maintain foot clearance. This action is controlled by the concentric contractions of the Sartorius, Rectus femoris and the iliopsoas muscles. During the swing phase the hip adductor muscles ensures energy efficiency by aligning the feet towards the path.

### **2.1.6 Abnormal Gait**

Abnormal gait is characterized as a behavior that deviates from normal gait due to different kinds of abnormalities / disorders. Abnormal gait is devoid of many significant gait functions like sensation, strength, coordination which are observed in a healthy (normal) gait.

#### **Etiology of gait abnormalities**

Clinical features of Gait disorders may be associated with neurologic or non-neurologic disorders. Common causes associated with non-neurologic include osteoarthritis lower extremities hip and knee, orthopedic deformities and visual loss [35]. Patients may experience an automatic reduction in stance time which occurs as a tendency to reduce pain in the affected limb, thus resulting in an asymmetric antalgic gait. Neurological disorders listed in Table 2.2 are described in further detail. Shortened step length, decreased velocity, increase in double limb support time, mildly shortened step length [36] are the significant gait parameters [37] seen in aged groups but are also seen as a response to instability, due to internal and external factors. Individuals may need to stretch their upper limbs in-order to attain stability resulting in a cautious gait or unsteady gait [36].

#### **Spastic Gait**

Spastic gaits are a result of unsteady motion caused by lesions in the corticospinal tract which may affect a single or both lower limbs. The affected limb is held in extension and plantar flexion; the ipsilateral arm is often flexed [36]. Circumduction of the affected leg develops during the swing phase of each step which is the significant sign of this gait. Common causes include stroke or other unilateral lesions of the cerebral cortex. Spastic gait may appear as stiff-legged or scissoring gait owing to increased tone in the adductor muscles, such that the legs nearly touch with each step when two limbs are affected.

#### **Neuromuscular Gait**

Muscle weakness of the lower extremities is considered as a neuromuscular gait disorder. Such type is called as waddling gait and can be seen in cases of proximal muscle weakness. In normal gait the glutens serve to stabilize the pelvis by uplifting the non-weight bearing side during each cycle. Weakness in these muscles specially the gluteus medius leads to excessive side trunk motion resulting in a waddling appearance [38].

Steppage gait is caused by weakness in ankle dorsi flexion, commonly known as foot drop. General behavior exhibited by individuals is lifting the swinging leg higher to compensate for the toes weakness to clear the ground during each cycle. Foot drop can also be bilateral, which can be seen in peripheral neuropathy or unilateral [36].

### Parkinson's Gait

Parkinsonian gait is one of the most common gait disorders seen in elderly individuals. A shuffling appearance caused by reduction in step length and height. Stooped posture, swinging arm and a narrow base to normal are the common behaviors (Figure 2.4). It is characterized by simultaneous rotation of the head, trunk and pelvis associated with a tremor unlike in normal gait where the head rotates first which is then followed by trunk and pelvis [39]. Step length, velocity, arm swing, and turning speed can be improved through proper medical treatments [40].

Gait Disorder(GD)	Number(Percentage)*	Total Number <sup>1</sup>	Causes(Number)
Single neurologic GD	81 (69.2)	46	Peripheral sensory neuropathy (46)
Sensory ataxic	22 (18)	46	Peripheral sensory neuropathy (46)
Parkinsonian	19 (16.2)	34	Parkinson's disease(18), drug-induced(8), other(4)
Frontal	9 (7.7)	31	Vascular disease(18), dementia(7), other(3)
Cerebellar ataxic	7 (6.0)	10	Stroke (3), multiple sclerosis(1),alcohol abuse(1), tremors(3), other(2)
Cautious	7 (6.0)	7	Idiopathic (7)
Spastic	6 (5.1)	7	Ischemic stroke(3), other(4)
Hypotonic	6 (5.1)	14	Nerve injury(5), other(3)
Other	5 (4.3)	10	Vestibular disease(6), dyskinetic(4)
Multiple neurologic GD	36 (30.7)		
Total	117		

Table 2.2: Prevalence of Neurological Gait Disorders in 117 Community-Dwelling Adults [31].

Freezing gait and festination [36] are features of more advanced Parkinson's disease. It

is defined as an inability to generate an effective stepping despite having an intention to walk [11]. Affected people feel a restrictive force opposite to their limb movement commonly seen while starting gait, turning, or approaching a destination but can also be motivated by external features, such as narrow hallways, doorways [41]. Freezing gait is a key cause to fall risk [42]. Freezing conditions can be improved with a regulated prescriptive dopaminergic medication.

Festination is a phenomenon in which steps become increasingly rapid and short, which appears close to running. The center of gravity moves forward. Festination may lead to freezing which is independent but also causes fall [43].

### Cerebellar Ataxic Gait

This gait is characterized by the irregular, uncoordinated movements of cerebellum called as ataxia. Cerebellar ataxic gait may manifest only as difficulty with tandem gait [44]; individuals tend sway or fall when requested to walk heel-to-toe. A severe form of this abnormality is wide-based (to compensate for instability), step length is variable, turns are unsteady, and there is frequent side-to-side lurching or deviation. Assistive devices such as a walker are generally suggested by physicians to reduce the risk of injury due to falls. Diagnosis of cerebellar gait ataxia may be narrowed by timely symptom onset; stroke is a common cause of acute ataxia, autoimmune or other inflammatory disorder, and neurodegenerative conditions or alcohol may cause chronic cerebellar ataxia. Imaging of the brain is typically necessary.

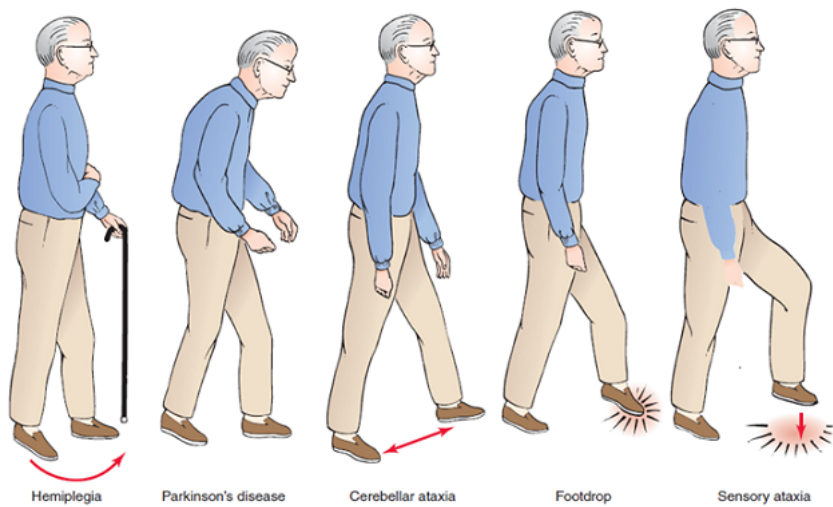


Figure 2.4: Pictorial representation of Classical Gait Abnormalities, taken from [31]

### Sensory Ataxic Gait

Discrepancies in sensing the position of limbs and joints also known as proprioception, which then resulting in an unsteady gait is known as sensory ataxic gait. The stance in this type is characterized by a wide -based and a short step length and a stomping quality as the foot hits the ground. Affected individuals often tend to look down at their feet as visual cues help them in compensating the proprioceptive deficits. Therefore, their gait worsens in dark environments or when they are asked to close their eyes [36]. Such kind of reflexes are improved with treatments such as physiotherapy [45].

### Frontal Gait

Most common higher-level gait disorder is the frontal gait. Higher-level disorders encompass a class of gaits that are completely different from the above discussed ones [19]. Weakened balance is the vital feature, and widened step width like in cerebellar and sensory ataxia. Variable step length and step height is diminished, failure to initiate gait is a prominent feature; feet appear glued to the floor when the subject tries to begin walking, a feature that may also occur in isolation and many other characteristics can be seen as explained in [46]. These features describe this gait as a class of gait that is “magnetic.”

Common causes are microvascular white matter diseases, neurodegenerative systems. For individuals with frontal gaits, recommended treatments are physical therapy and assistive devices to decrease fall risk.

### Gait Parameters of Abnormal Gait

Human gait parameters shown in Table 2.1 provide a scope for a comparative analysis in-order to differentiate normal and abnormal gait behaviors. Reliability of several of these gait parameters has helped us for a reasonable comparison to classify as normal and abnormal gait. Several of these parameters are briefly described here :

*Normalized Peak pressure (NPP) :* It is the ratio of peak value of foot plantar pressure and the subject's body weight. Two peak pressures commonly appear in one cycle in stance phase (heel-strike and toe-off)

*Foot-flat ratio (FFR) :* Foot flat ratio is defined as the fraction of stance phase for which the foot is in contact with the ground. To compute FFR the ratio between flat foot duration and stance phase duration is considered.

*Stance ratio:* Time duration of two adjacent heel-strike events is defined as step time. The cycle time divided into stance and swing time. The stance ratio is defined as the ratio between stance time and step time.

*Step-time variability:* The standard deviation of step time is used as its variability.

*Stride Length:* Stride length is the distance between two successive heel-strokes of the same foot.

*Cadence:* It is defined as the rate at which a person walks, expressed in steps per unit time.

Computation of these gait parameters for classification of normal and abnormal gait is explained in Chapter-5.

### 2.1.7 Summary

Functional gait disorders are formerly referred as psychogenic which are typically abrupt in onset and also fluctuate over time. Common indications are excessive slowing of gait or weakness, usually without falls. Gait disorders are mainly caused due to disability, morbidity and mortality mostly in elderly individuals. This chapter has provided an overview of the features of various gait abnormalities , focusing on the characteristics that play a vital role for recognition, effective intervention and improvement through various treatments prescribed by neurologists and psychiatrists.

## 2.2 Inertial Measurement Units

Inertial measurement units (IMU's), also called as inertial sensors are used to measure acceleration, angular velocity and magnetic field in any local coordinate system. Generally, these sensors are attached to a rigid surface calibrated in-order to estimate the orientation, acceleration of a particular object with respect to its axis.

The use of IMU's for human motion analysis has helped many researchers in the field of bio-mechanics to obtain quantitative measure of motion parameters of their patients. Currently, there is a significant growth in using these sensors especially in application domains ranging from clinical, sports, recognition, rehabilitation and game development. In the following, we will briefly review few concepts of IMU's such as error characteristics and algorithms that are used in Chapter-3 to compensate such errors so that accurate estimates can be computed.

### 2.2.1 MEMS Gyroscopes

Gyroscopes measure angular velocity with respect to an inertial frame of reference. The sensing mechanism is based on Coriolis effect [47], which is defined as, a mass  $m \in \mathbb{R} > 0$  moving with a velocity  $v(t) \in \mathbb{R}^{3 \times 1}$  with respect to a coordinate system, that rotates at an angular rate  $g(t) \in \mathbb{R}^{3 \times 1}$  experiences a force  $F_c(t) \in \mathbb{R}^{3 \times 1}$  denoted as,

$$F_c(t) = 2m(v(t) \times g(t)) \quad (2.1)$$

where the  $\times$  is a vector cross product operation. The measurement principle shown is only for one coordinate axis (with scalar velocity  $v(t)$ , angular rate  $g(t)$  and force  $F_c(t)$ ) in Figure 2.5. Three-axis gyroscope, three of those respective single-axis units are mounted perpendicular to each other. To compensate for mounting inaccuracies, an orthogonal matrix is calculated during calibration and then applied to the measurement output vector.

### 2.2.2 MEMS Accelerometers

Accelerometers contain a mass element that is suspended by a spring, such that the element is displaced whenever it experiences an amount of force in the form of displacement. In conventional accelerometers, the displacement is directly measured. The former one is depicted in the Figure 2.6 below.

When an accelerometer is at rest or in motion at a constant velocity, the mass element is affected only by gravity, the gravitational pull towards the earth's center. In such cases the measured value is equal to  $9.8\text{ms}^{-2}$  directed vertically upwards. When in motion, the measurement equals to the sum of his gravitational pull and the relative change in velocity.

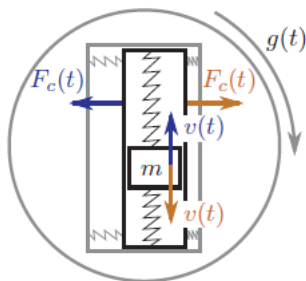


Figure 2.5: Coriolis effect to measure angular velocity: Oscillation of the mass  $m$  produces another perpendicular oscillation. After calibration, the absolute value of the angular rate can be computed from the oscillation amplitude, while the phase difference between both oscillations yields the direction of rotation [42].

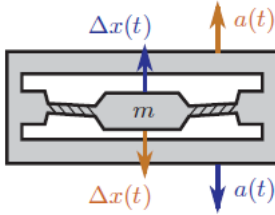


Figure 2.6: Principle of an accelerometer where the mass  $m$  is suspended in such a way that it can oscillate up and down along the axis. When accelerated, the device causes a displacement of the mass with respect to the enclosure [42].

### 2.2.3 Error characteristics

When an accelerometer or a gyroscope are not undergoing any acceleration or rotation, an ideal measurement output should be equal to zero or  $g$  which is  $9.8ms^{-2}$ . In practice, an offset from these ideal values will be measured and an average of these offsets is called a bias.

Integrating an IMU signal affected by a non-zero bias over time, results in an error that grows linearly with respect to time. This phenomenon is defined as drift [47]. Generally, the bias is subtracted from the obtained output a standard procedure carried out during calibration of the sensor module. However, calibration procedures are not accurate and only approximate the bias error where a complete bias compensation is not achieved. An excellent work by [48] gives an in-depth insight of the error characteristics in IMU's.

In order to compensate the uncertainties experienced by gyroscopes and accelerometers, the following algorithms are proposed. Kalman filter was employed in-order to filter the high and low frequency noises which gave accurate readings from the inertial sensors. Detailed information of the algorithms is explained below.

### 2.2.4 Complementary filter

Complementary filters can be used to combine two measurements of a common signal with different noise levels to produce a single output. High pass filter is generally used on a signal with low frequency noise, while low pass filter is used with another signal containing high frequency noise. The subsequent transfer function [49] applied to the signal is represented in equation 2.2

$$H(s) = H_{LP}(s) + H_{HP}(s) \quad (2.2)$$

This has the advantage that no group delay is applied to the signal. As explained the rate gyroscope integration suffers from low frequency drift, vector observation method suffers from high frequency from high frequency movement errors i.e., it is accurate only for slow moving objects. The formulation of the complementary filter defined as in equations 2.3, 2.4

$$q(t) = q'(t) + \frac{1}{k}(q''(t) - q'(t)), |a - 1| < a_T \quad (2.3)$$

$$q(t) = q'(t), |a - 1| \geq a_T \quad (2.4)$$

### 2.2.5 Kalman filter

Kalman filtering predicts the future state output given the current state and set of control inputs. The system process is defined by the following formulations [50], state equation 2.5 and output equation 2.6

$$X(k+1) = Ax(k) + Bu(k) + w(k) \quad (2.5)$$

$$Y(k) = Cx(k) + z(k) \quad (2.6)$$

Where x is called the system state,k is the discrete time index,A, B, C are matrices; A is called the state transition matrix, B is a matrix relating to control inputs, C is called observation matrix relating to the state of observations.u is the input to the system, y is called the measured output. The variables w and z are noises; w is process noise and z is measurement noise. There are various models of Kalman filter used for sensor fusion of inertial sensors which differ in state vector size and preprocessing steps.

## 2.3 Plantar Pressure Systems

The pressure field that is present between the foot and the support surface is termed as foot plantar pressure. This pressure field is also referred to as Ground Reaction Force (GRF). Acquisition of pressure information is important for gait and posture research, mainly gait phase detection and step detection [51–53]. The sensors translate the GRF into a proportional current or voltage.

Unlike inertial sensors which have axes components, plantar pressure sensors don't account for the components of the force measures on all axes. Compared to floor sensor systems, wearable in-shoe sensors are flexible, portable and allow data collection in various terrains. Therefore, allowing a wider variety of gait studies [54]. The pressure sensors are generally of the types – capacitive and piezo-resistive [55]. The selection criteria are based on robustness, range, linearity, sensitivity, and reliability. For reliable data sensors need to be secured suitably as there is a possibility of slippage of sensors. Although floor sensor systems have better spatial resolution compared to in-shoe systems, there has been constant improvement in shoe pressure measurement systems. One such system is described in the figure below 2.7. The reliability and repeatability have also an important role to play in the sensor choice [56].



Figure 2.7: Commercial plantar pressure insole developed by Tekscan [56]

When compared to the floor sensors, the Smart Insoles offer the possibility of segmenting the plantar regions of the foot. This segmenting action would help in making a more detailed analysis. This sensor is also been used for creating dynamic pressure maps of the plantar force changes which could mark regions of peak pressure. This information is unachievable in case of the floor sensor platforms.

The centre of pressure and ground reaction force could also be isolated by region of the foot, hence advancing the analysis of the foot function. Due to these abilities the pressure mapping of the foot is considered as a significant part of bio-mechanical analysis. Figure 2.8 illustrates the foot mapping technology presented by Tekscan. The studies by Tekscan also describe the capability of a single sensing unit to assess many crucial parameters of gait. Developments in wearable technologies have also made them affordable and accessible.

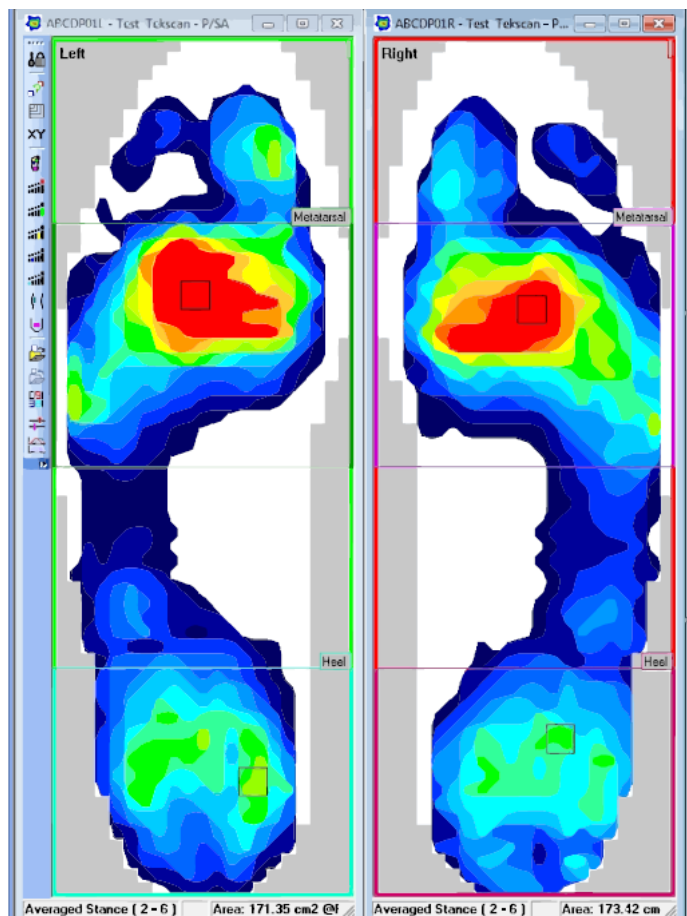


Figure 2.8: Plantar pressure mapping developed by Tekscan [56]

## 3 Hardware, Data Logging and Visualization

### 3.1 Hardware System

The backbone of a successful gait analysis system is the hardware system and a low-level user interface written in java script that performs the data collection. In this thesis, the role of the developed hardware system consisting (i) Sensorized In-sole measuring Plantar pressure, (ii) IMU's measuring the segment orientations, were designed and developed to satisfy the following goals and requirements:

- *Piezo-Resistive:* Emphasis was given in designing piezo-resistive based sensorized insoles. A detailed integrated research project on the choice of piezo-resistive materials was carried out prior to this thesis.
- *Gyroscopic uncertainties:* The IMU modules developed are robust from gyroscopic uncertainties, placement of these modules at any location on the segment joints do not impact the performance of the sensor modules.
- *Data Acquisition:* Multiple streams of data from the sensors was collected using TCP/IP protocol over W-LAN at an average frequency of 30ms. Though the data was collected in an asynchronous manner, the frame format of the TCP/IP protocol and the average bandwidth gave us an advantage in flawless data acquisition.
- *Time-stamped Asynchronous Data Logging:* Recording all the sensors and data streams using the timestamps as a centralized feature that allows perfect synchronization of the multiple data streams in post-processing.
- *User Interface:* A user interface was designed in-order to visually guide the user throughout the data collection process. Easy interaction with the hardware enabled the user for a timely collection of the data (start and stop times). Information such as user's Name, Age and Weight were asked for further data analysis.
- *Form Factor:* Parts of the hardware system have a small form-factor and the characteristics of the materials used do not impact the overall performance and also do not impact the activity performed by the individual.

Since the objective was to design an instrumented insole with Piezo-resistive materials and after few prerequisite studies, number of piezo-resistive based sensors were theoretically investigated prior to this thesis. The design was focused in-order to monitor wider areas to get a good resolution / visualization of the pressure mappings. The developed system uses common components customized to suit its requirements achieving a scalable cost effective, accurate, extendable and robust data recording platform. A detailed description of the components employed in the development of the In-sole are discussed below

- **Pressure conducting fabric**

A Pressure conducting fabric manufactured from Eeontex [51], see Figure 3.1. Fabrics manufactured by Eeontex are smart fabrics coated/doped with an inherently conductive polymer also called E-textiles, making them conductive with quite high resistance



Figure 3.1: Pressure conducting fabric manufactured by Eeontex, works on the principle of piezo-resistive functionality

The resistance of these fabrics varies subjective to the pressure applied through the material, and stretch over the material making them ideal for sensor construction. This Eeontex smart fabric is a conductive, non-woven microfiber with piezo-resistive functionality for use in dynamic sensors to map and measure pressure, bend, angle, stretch and torsion [69]. Characteristics of the pressure conducting fabric used in this thesis are tabulated in table 3.1

Property	Quantity
Dynamic Range	5g - 100kg
Dynamic Response	500 cycles/sec
Density	170g/m <sup>2</sup>
Thickness	0.80mm
Surface Resistance	2K ohms/q

Table 3.1: Characteristics of Eeontex Pressure conducting fabric

- **In-sole Layout**

Sensorized matrix structure [49] with copper electrodes, see Figure 3.2 and 1mm Ethyl Vinyl Acetate (EVA) foam sheets to enclose the assembly design which acts as a substrate enclosing the sensor material from both ends.

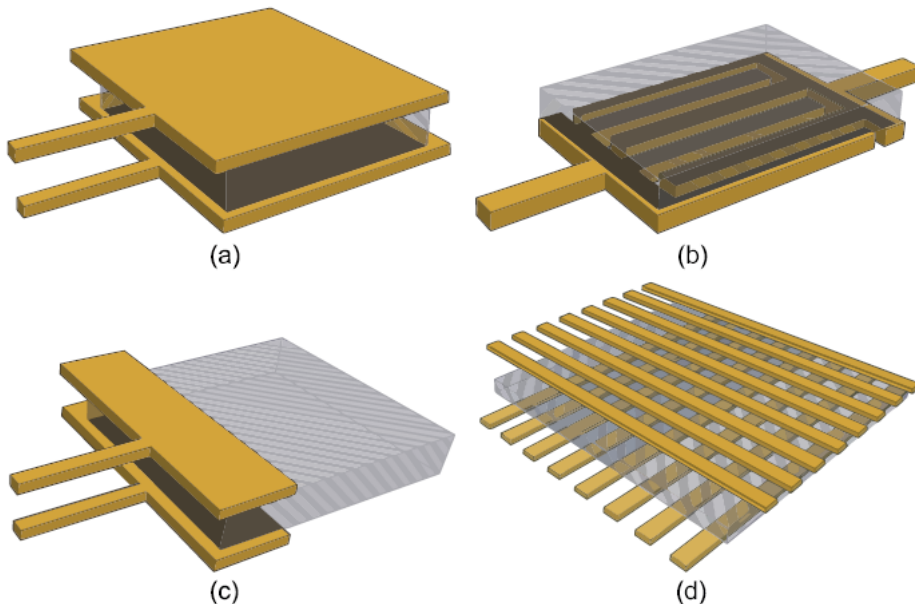


Figure 3.2: Common sensor structures, conductive copper electrodes are in yellow; polymeric sensor material is in transparent gray: (a) single point sensor structure, (b) single point sensor inter-digital structure, (c) single point sensor fringe electrode structure, and (d) sensor matrix. Sensor matrix structure was designed in this thesis after carrying out several tests regarding homogeneity, repeatability, linearity and hysteresis.

Matrix structure shown in Figure 3.2 (d) was designed, the insole assembly with horizontal and vertical electrodes where Ribbon cables are used for the connections of the horizontal and vertical electrodes. The matrix takes form of 63 nodes in total containing 15 horizontal and 5 vertical electrodes in shown in Figure 3.3



Figure 3.3: Insole assembly, with copper electrodes on eva foam substrates and the Eeontex sensing fabric in the center

- **Circuit components**

A Conditioning circuit to obtain the output proportional to the fabric's resistance. 16 channel Multiplexer (74HC4067N) connected to an ESP-32 micro-controller so that resistance across each sensing node could be calculated. The circuit was powered using a 3.7 V Lithium-Polymer batteries, when fully charged enabled the device to run for longer periods. The whole assembly was designed and fabricated on a PCB board. The schematic is shown in Figures 3.4 and 3.5

Inertial sensors were used for quantitative assessment by estimating the orientation of the lower limbs (segments or joints) and angle as a unit of measure to characterize human gait activity. Figure 3.6 depicts the position of sensors placed on the segments which gives a clear picture of the objective. Note that the project focuses only on assessing the segments of lower limbs. The components used in development of Inertial sensor modules are detailed below

- **MPU-9250**

A second generation Motion Processing Unit (MPU) developed by InvenSense. This is the smallest 9-axis MPU that combines 3D accelerometers, 3D gyroscope and 3D magnetometer. It contains a DMP unit used to process the complicated motion fusion algorithms. The breakout board module of the MPU-9250 has been developed for ease of experimental analysis. A micro-controller was interfaced

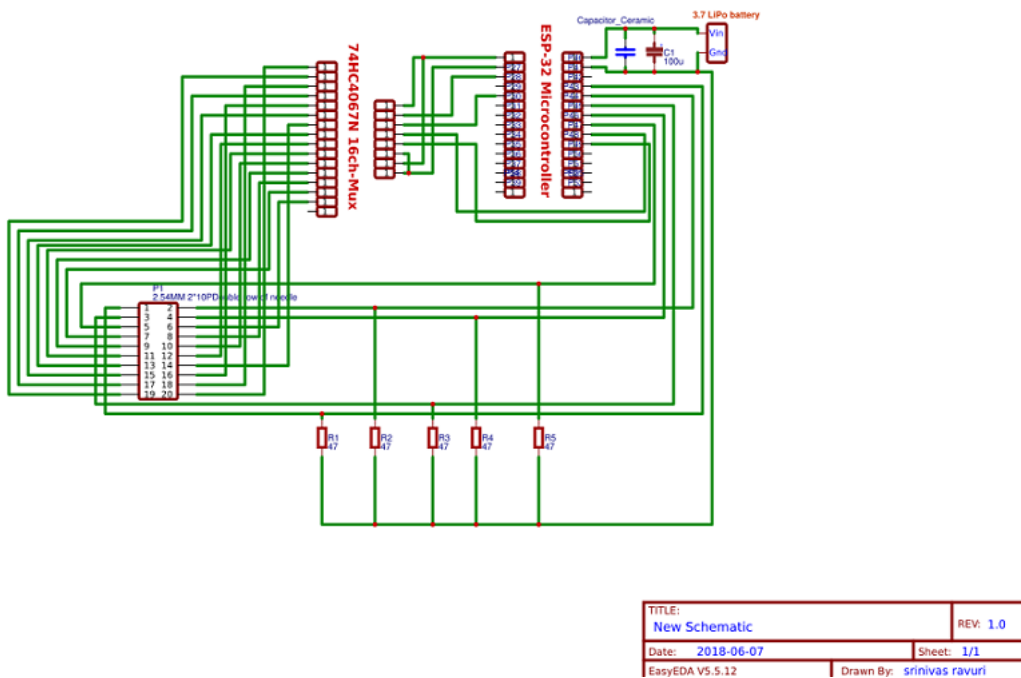


Figure 3.4: In-sole circuit schematic designed using EasyEDA

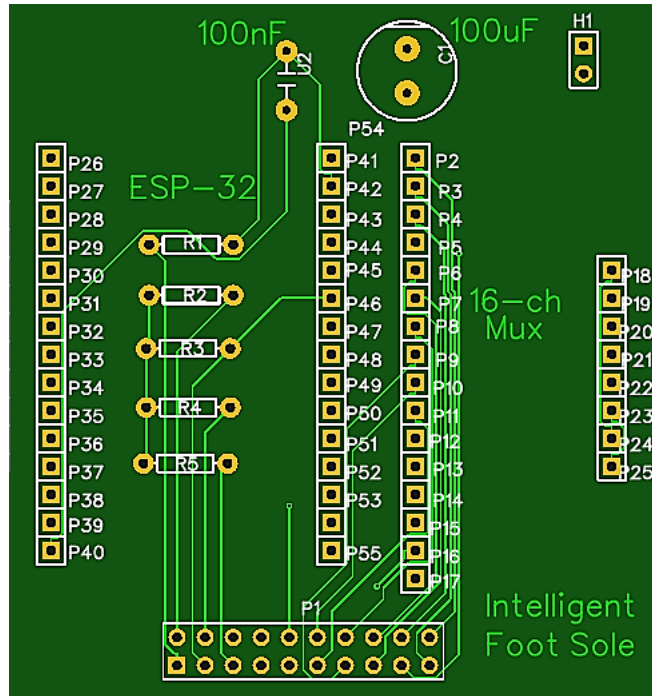


Figure 3.5: Printed circuit board mid-assembly showing populated positions of ESP-32 controller, 16-ch Multiplexer, bias resistors (R1 to R5), JTAG connector interface (P1) and LiPo power source connector (H1). Also not shown are positions for the power switch and LiPo batteries

with the MPU-9250 module. Fully assembled IMU sensor module containing the ESP-8266 micro-controller, MPU-9250 module, Li-Po battery along with common components(such as capacitors and resistors for voltage regulation).



Figure 3.6: In-shoe plantar pressure sensor and the printed circuit board fabricated into an enclosure(left), Sensor setup on the subject (right)

The final prototype versions of the Pressure sensing insole and the Inertial sensor employed in an enclosure are shown in the Figure 3.6.

## 3.2 Data Acquisition

The Data acquisition system consists of sensors, measurement hardware for data collection and a programmable software. Compared to conventional measurement systems, PC or mobile based data acquisition systems can better utilize the processing power, productivity, display capabilities, and connectivity especially for applications such as gait analysis, providing a more powerful, flexible, and cost-effective measurement solution. Therefore, a mobile based UI (user-interface) was developed using Java script where the individual has complete flexibility while interacting with the software. Information such as age, weight and height which are considered to be significant parameters for data analysis were also taken from the subject. The complete picture of the developed user interface is shown in Figure 3.7

The acquisition process is as follows:

- *First step* is regarding the subject's information such as age, weight and height which have to be entered in the respective fields as shown in Figure 3.7(a). The transcribed details are then used for further analysis.
- *Second step*, a 20 seconds count down timer starts as soon as the user clicks the start button after giving his details. This timer allows the user to prepare himself for the experiment and also the latency gives us an advantage to synchronize the multistream data during post processing. The Figure 3.7(b) depicts the second step

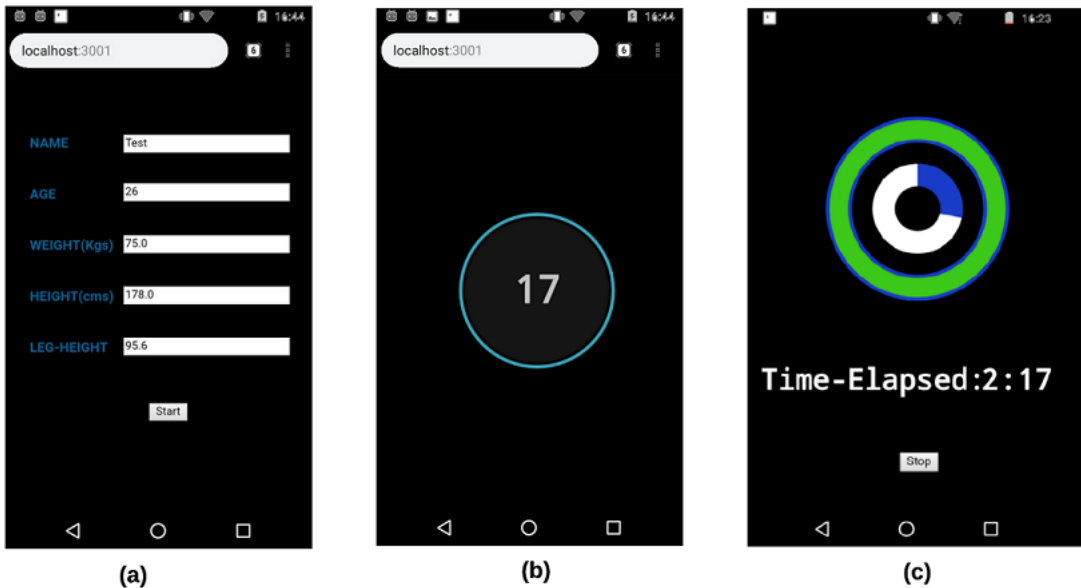


Figure 3.7: User Interface programmed using Java-script, Independent of the device OS version, it is a browser compatible interface can be deployed in any of the modern Android smart phones. Currently running on Android 6.0 (Marsh mellow): (a) First step, user details screen with start button (b) Second step, 20 sec count down timer (c) Third step, Elapsed time screen with stop button

of the data acquisition process.

- *Third step*, the user starts performing the activity as soon as the instructions appear on the screen and a timer starts ticking see Figure 3.7(c) recording the elapsed time of the activity performed. A stop button is programmed which ensures the completion of the experiment. Here, the user has flexibility to stop the process if he is disturbed by any internal or external factors by clicking the stop button.
- *Fourth step*, the final step of the data collection process. As soon as the user clicks the stop button, Figure 3.7(c) the data is logged into individual files respective to each sensor, saved within the device's memory. This completes the data acquisition process.

A complete block diagram of the data acquisition process is depicted in Figure 3.8. The start button triggers the recording of the data from the TCP/IP-clients which are the sensor modules. Data is collected at a frequency of 30ms, though the transfer rate varies among the clients the 20 seconds latency programmed in the UI (step-2) is used here to synchronize the data during post processing. The collected data contains individual files of pressure and orientation information ( processed with Kalman and Complementary filter on Accelerometer and Gyroscope Information) respective to each limb. The TCP/IP-server collects the information logged by the clients and as soon as the stop button

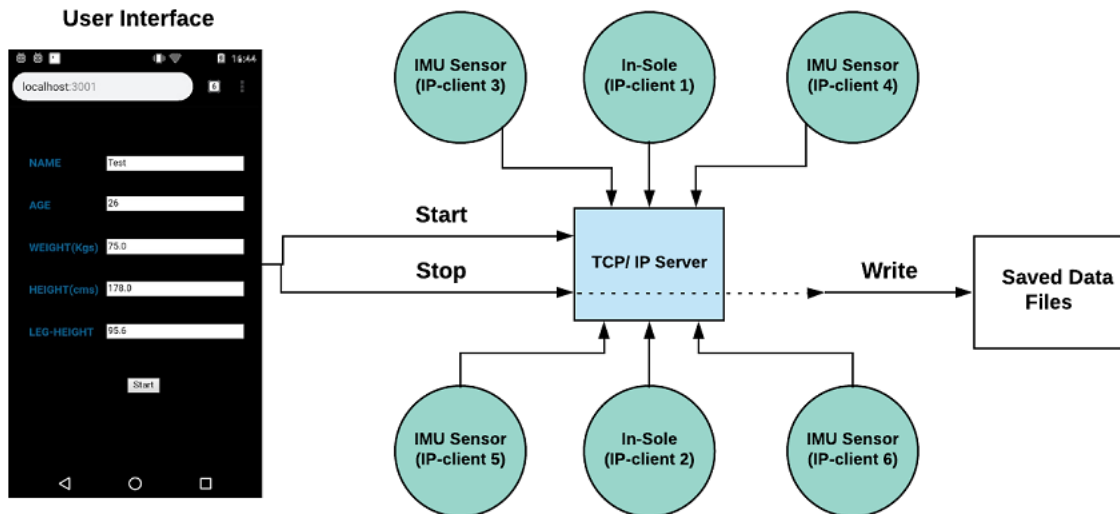


Figure 3.8: DAQ block diagram showing the TCP/IP client - server operations controlled by the user interface. The data is stored into log files in text format.

is pressed, the data stored in the buffer of the server is written into log files and stored within the device memory. The data files are the end point of the data acquisition process shown in block diagram Figure 3.8. The block includes numerous TXT files that provide time stamping information and raw sensor data information.

### **Left and Right In-sole.txt**

Contains timestamp, plantar pressure information segmented into regions depicted in Figure 3.9. The txt files are saved along with the user information.

### **Left and Right Shank.txt**

Contains timestamp, accelerometer, gyroscope, kalman filter and complementary filter calculated orientations for the shank segment.

### **Left and Right Thigh.txt**

Contains timestamp, accelerometer, gyroscope, kalman filter and complementary filter calculated orientations for the thigh segment.

### 3.3 Data Visualization

The pressure distributions are unique to each individual and vary based on several factors such as gait velocity, body weight, age, foot shape and stride length. However, walking pacing and the structural changes in the foot's arch could significantly influence the plantar pressure distribution. Therefore, the plantar surface of the foot is subdivided into eight different anatomical regions [56] -M01 (heel region), M02 (medial mid-foot), M03 (lateral mid-foot), M04 (medial fore-foot), M05 (central fore-foot), M06 (lateral forefoot), M07 (hallux region) and M08 (toes). These regions help in a detailed investigation of the pressure distributions.

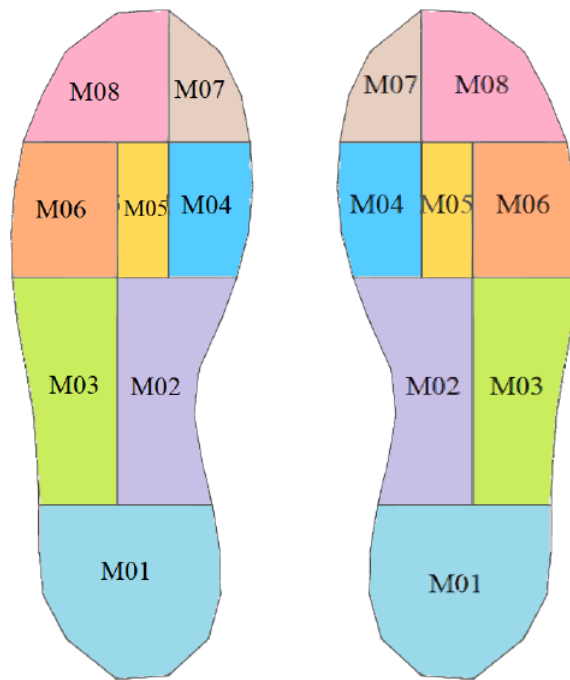


Figure 3.9: Foot anatomical regions, M01 (heel region), M02 (medial mid-foot), M03 (lateral mid-foot), M04 (medial fore-foot), M05 (central fore-foot), M06 (lateral forefoot), M07 (hallux region) and M08 (toes)[115]

The pressure distribution on the plantar region of the foot is also affected by the abnormalities discussed in Chapter-2. Previous studies have shown that the pressure under the plantar surface increases during the foot movement especially on the rear mid foot and lateral mid foot. Also, the shape of the foot impacts the severity of the gait disorder as shown in [56]. The segmented anatomical regions shown in Figure 3.9 give an advantage for more detailed analysis of the pressure patterns which help in diagnosis of the gait disorders prior to their occurrence. Each anatomical region has its own significance, especially in terms of analyzing gait abnormality.

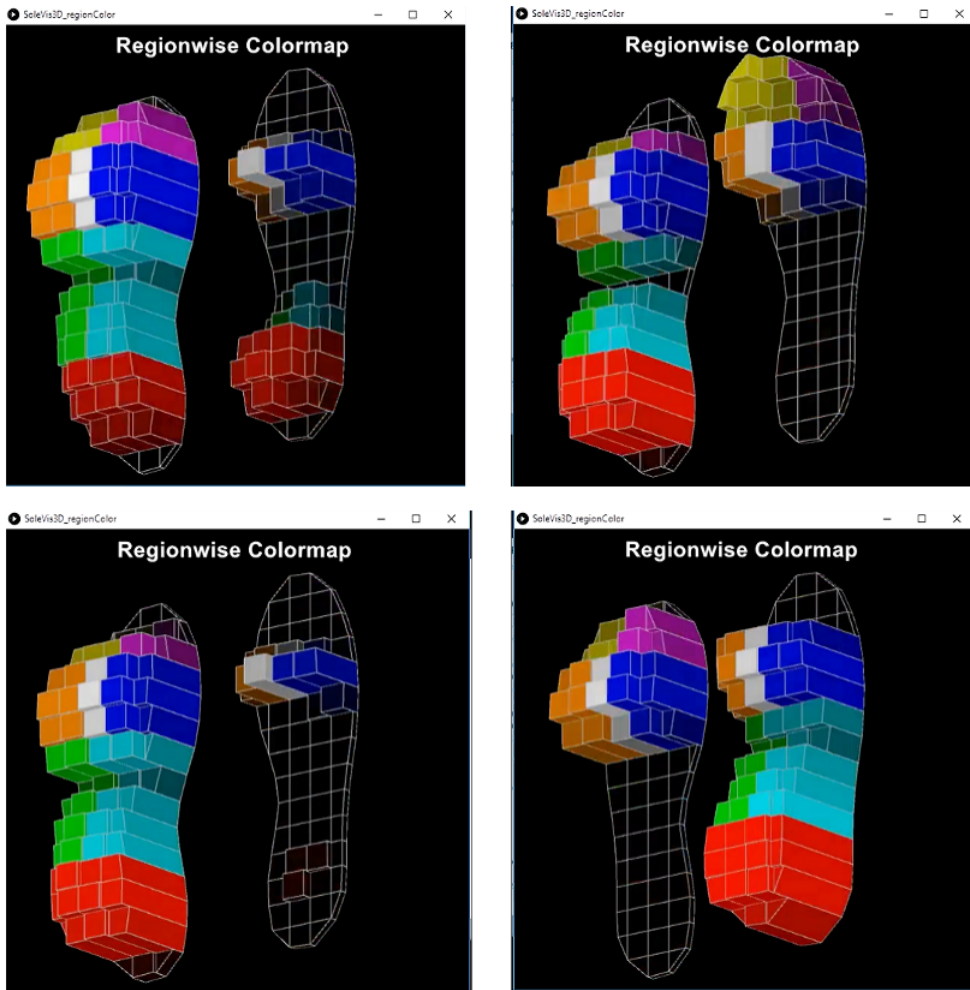


Figure 3.10: Visualization of quantitative pressure measured from the custom built pressure sensing insole based on piezo-resistive methodology. The segmented regions are populated with varying color system correlating to the sensor value.

Visualization of quantitative pressure information collected from the anatomical pressure regions is visualized in a 3D In-sole graphic programmed in Processing IDE (Processing 3.0, MIT, USA). Visualization is depicted by correlating the sensor value in respective cells and populating the cells in the insole with varying color system. The color in each cell is definite with series of formulae, each depicting a color. By placing the formulated value in respective cells, we were able to achieve the desired color representing the Amount of pressure magnitude in various locations. Figure 3.10 depicts qualitative plantar pressure region based visualization. Visualization of plantar pressures of different abnormal gaits and significant anatomical regions respective to each abnormality are discussed in the next chapters.

## 4 Machine Learning based Gait Analysis

### 4.1 Introduction and Motivation

Machine Learning methods have been extensively used in the context of gait analysis, estimating various spatial and temporal parameters that are used for gait assessment. Modern machine learning techniques have outperformed and complemented the use of conventional statistical methods in bio-medical systems. In this chapter, we present a review of the machine learning techniques that have already been deployed in the context of gait analysis and the framework adopted in this thesis in-order to calculate the gait parameters explained in section 2.1.6

### 4.2 Related Work

Research on using artificial neural networks for to determine gait events such as initial contact and end contact using six accelerometer sensors positioned along the legs was presented by Mijailovi et al. [16]. The relative error reported was 11% for intra-subject and 14% for inter-subject estimations. Extraction of gait parameters with Deep convolution neural network was presented by [18].

A machine learning framework to identify specific diseases associated with neurological disorders using gait analysis data was presented by [57], where the authors use three different types of machine learning algorithms: Random Forest, Support Vector Machines and Multi-layer Perceptron. Reported classification accuracy was 100% with cross-validation. The authors also report, reducing the number of features used for classification in order to further decrease computation time and algorithm complexity as future research. Neural network-based gait assessment, estimating gait parameters like joint angle, joint force, and joint moment using the ground reaction forces (GRFs) and moments was proposed by [58].

Arosha et al. [59] investigated on identification of gait patterns with neuromuscular signals and soft tissue deformation analysis of lower limb muscles using an Artificial neural network. A novel artificial neural network based method for real-time gait analysis for accurate lower limb attitude estimation in clinical gait diagnosis for orthopaedic patients

and patients with neurological diseases was proposed by [60]. Most of the research groups used algorithms such as Support vector machines, Hidden Markov models, Artificial neural networks, Clustering techniques.

After a detailed literature survey, considering the amount of computational power required, reported accuracy of the models, computational time, robustness and reliability of the algorithms we propose a methodology in this thesis applied for segmentation of human gait to estimate gait parameters used for comparative analysis, shown in the later sections

## **4.3 Methodology**

In this section, we propose a methodology to classify human gait by utilizing the features acquired from the developed wearable sensor system.

### **4.3.1 Data collection and Preprocessing**

Data acquisition procedure explained in section 3.2 was followed and the experiments were conducted with 10 healthy individuals, the procedure of the experiment was first explained to the participants and two inertial sensors are attached on the thigh and shank on both limbs, the pressure sensing insole was placed into respective foot wear and the designed hardware was fabricated into an enclosure shown in Figure 3.6.

The participants were allowed to complete a natural walk of 10 meters as they would do in daily life. The layout of the environment in which experiments were conducted is shown in Figure 4.1.

Gait information collected from the participants contains segmented region based plantar pressure information, orientations of thigh and shank from the inertial sensors with respective time stamps. We use the time stamp information as a centralized feature to synchronize the data taking the advantage of the 20 second latency during the second step of the data acquisition process explained in section 3.2. The raw data collected in the form of text files is visualized as shown in Figure 4.2

Conventional techniques such as data normalization and data augmentation by adding Gaussian noise were used for preprocessing. The features containing significant plantar pressure regions that contribute most for characterization of human gait were used. Raw orientation measures of thigh and shank segments were preprocessed using a butter-worth

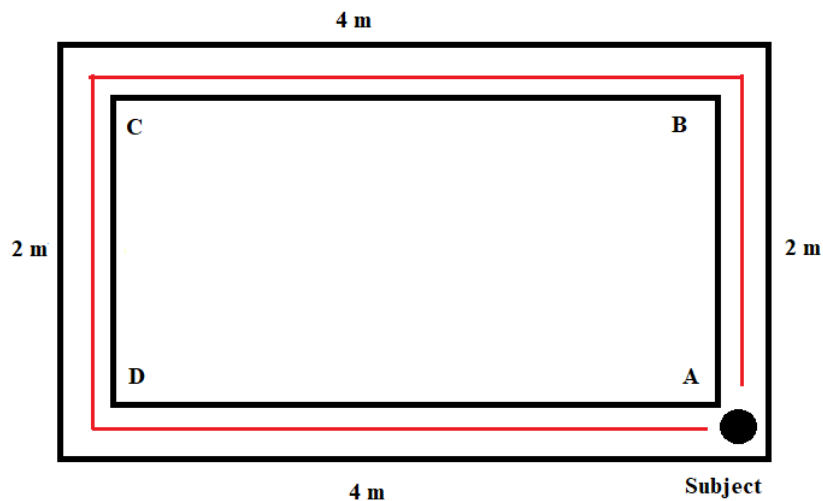


Figure 4.1: Walking path; A to D and back to A, A to B (normal speed), B to C (increased speed), C to D (normal speed), D to A (increased speed)

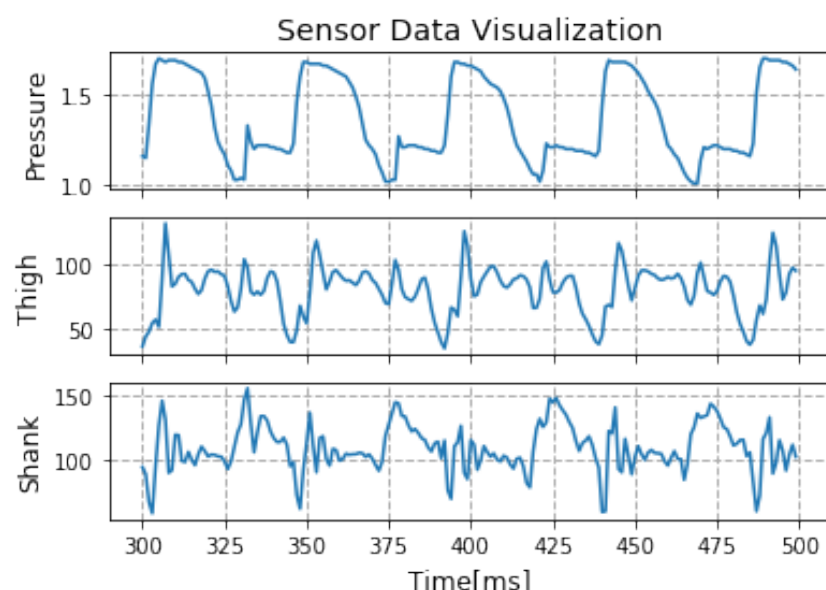
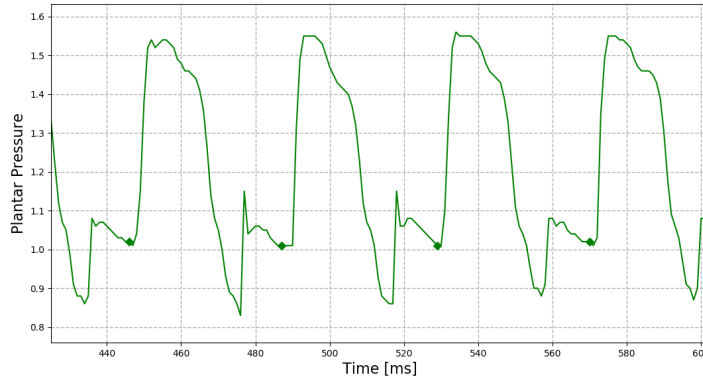


Figure 4.2: Visualization of raw information collected from the sensor system, from top  
Plantar pressure, thigh orientation and shank orientation in degrees

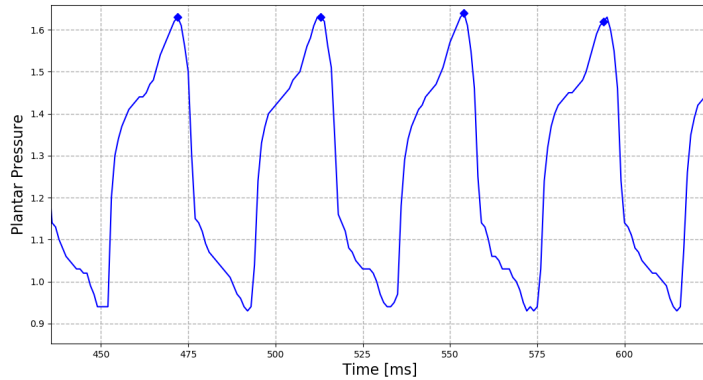
second order filter which gave an advantage in filtering the uncertainties as shown in Figure 4.4.

### 4.3.2 Data Annotation

The next step in the proposed framework was annotation of the preprocessed sensor data. The valleys of plantar pressure region M01, refer Figure 3.9 give us information regarding the start of the stance phase which is 60% of a gait cycle. Similarly, the peak value of plantar region M07, refer Figure 3.9 give information regarding the end of stance phase/start of swing phase which is 40% of a gait cycle. Therefore, by detecting such peaks and valleys, we were able to get information regarding the start and end of the stance and swing phases.



(a) Pressure data of plantar region M01; here the marked valleys represent start of stance phase (initial contact)



(b) Pressure data of plantar region M07; here the marked peaks represent start of swing phase

Figure 4.3: Annotation of input data; valleys as stance phase, peaks as swing phase

Also, the temporal difference between the detected peaks and valleys coincide with the standard RLA terminology [1] followed in this thesis.

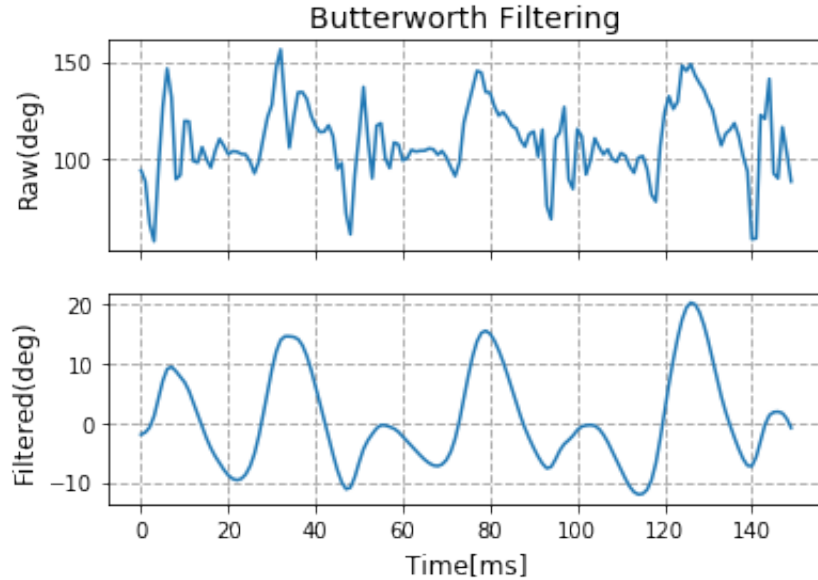


Figure 4.4: Preprocessing of segment orientations using Butter-worth 2<sup>nd</sup> order filter. Also the visualized graph is normalized.

### 4.3.3 Gait Phase Classification

#### Network Architecture

We train a Deep neural network (DNN) using the preprocessed dataset of the first group to classify the samples in the time series into subsequent phases. The input sequence contained multi-dimensional sample features plantar regions( M01,M07), thigh and shank orientations in each step of an epoch. Figure 4.5 shows the high-level architecture of the model. The training sequences are divided into three sets: train ( $t_n$ ), validate ( $v_n$ ) and test ( $n_t$  ).

The preprocessed feature vectors are passed through the feed-forward artificial neural network for classification. The classifier, based on its characteristics, maps the given feature vector into each of the two possible classes (Stance and Swing). The network, which is used as the primary classifier, is composed of multiple nodal layers which are interconnected and the architecture is such, that every individual node or neuron consists of a rectified linear unit (ReLU) activation function [61]; where  $x$  is the input.

$$f(x) = x^+ = \max(0, x) \quad (4.1)$$

For training, we use the Cross entropy loss function. Given the ground truths,  $y = [y_1, y_2, \dots, y_N]$  and the predicted output vector by the model,  $\hat{p} = [\hat{p}_1, \hat{p}_2, \dots, \hat{p}_N]$  the loss

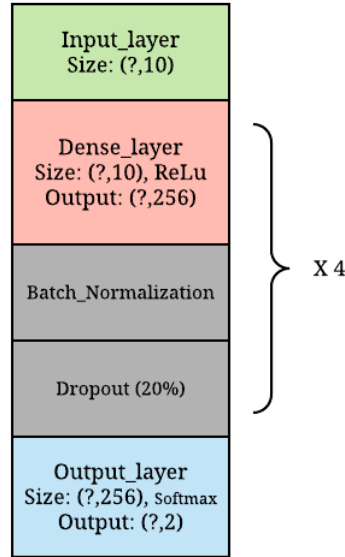


Figure 4.5: Architecture of the proposed DNN with 4 deep layers, the input features are the 8 plantar regions, thigh and shank segment orientations, output layer with shape of two classes

function is calculated as

$$L_{\log}(y, p) = -\log \Pr(y|p) = -(y \log(p) + (1 - y) \log(1 - p)) \quad (4.2)$$

A deep neural network (DNN) is an artificial neural network (ANN) consisting of multiple hidden layers. The DNN learns to find the correct mathematical relationship between the input and target variables in a linear/ non-linear fashion through a process called Back-propagation. The network moves through the deep layers calculating the probability of each output. Each mathematical manipulation as such is considered a layer, and complex DNN have many layers, hence the name "deep" networks.

Deep architectures include many variants of a few basic approaches. Each architecture has found success in specific domains. It is not always possible to compare the performance of multiple architectures, unless they have been evaluated on the same data sets. Training a DNN involves tweaking of many hyper parameters and in order to reduce the amount of complexity and time in tweaking the parameters we use a genetic algorithm to generate highly accurate and optimized results.

By applying genetic algorithm [62] we attempt to evolve a DNN with optimal hyper-parameters that help us in reducing the time spent on tuning the parameters through brute force trial and error approach. We try to find the best hyper parameters: Number of layers, Neurons per each layer, Activation in Dense layers, Epochs and Network optimizer.

The steps of the genetic algorithm are detailed below:

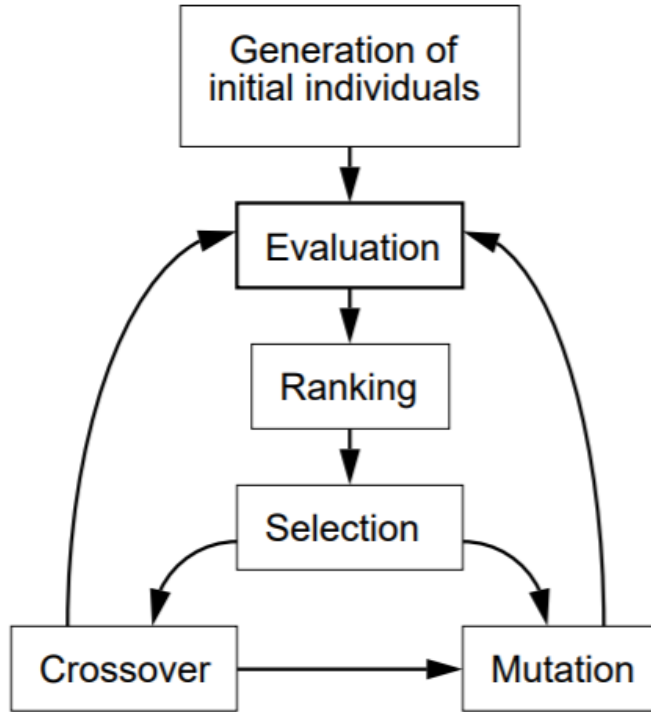


Figure 4.6: Genetic algorithm evolution process

- $N$  random DNN are initialized to create our population. Here we initialized  $N = 5$ .
- The classification accuracy of each  $N(N=5)$  networks is considered as a fitness function.
- All the networks are sorted based on the classification accuracy. Some percentage (50%) of the top networks become part of the next generation and are used to breed children.
- Mutation is carried out among some of the hyper parameters.
- We take two members of a population and generate one or more child network, where the child network represents a combination of its parents networks.

## Classification Results

The above steps are iterated continuously until we get the very best possible members of a population. After end of each iteration a new generation is formed. Through this we reduced our parameter tuning time by almost 80% assuming it found the best hyper-parameters.

The best hyper parameters given by the genetic algorithm after evolution of five generations are **Number of layers = 4**, **Neurons = 256**, **Activation = ReLu**, **Optimizer = Adam**. We plug these hyper-parameters into the model and the training progress of DNN on  $t_n$  and  $v_n$  is shown in Figure 4.7. The model achieved a 98% classification accuracy on  $n_t$ . The classification output of the DNN is visualized in the Figure 4.9

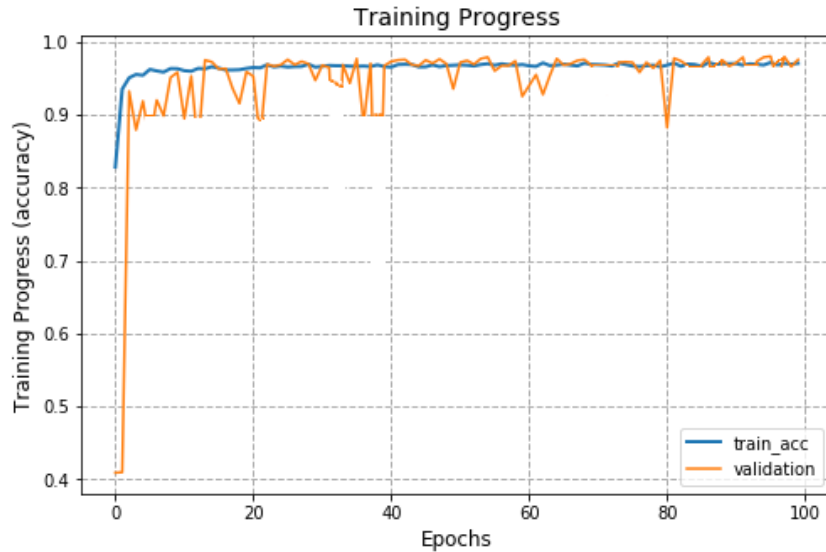


Figure 4.7: Model Training Progress (accuracy)

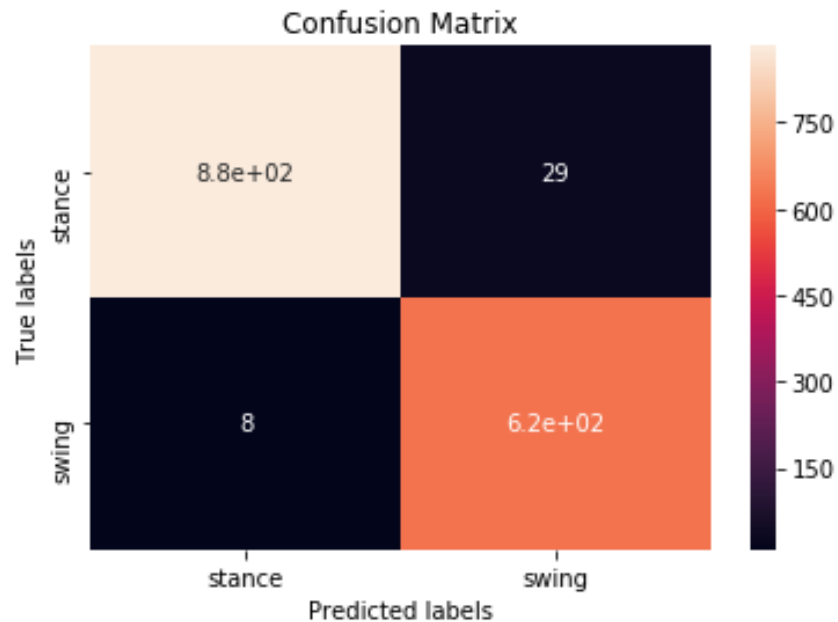
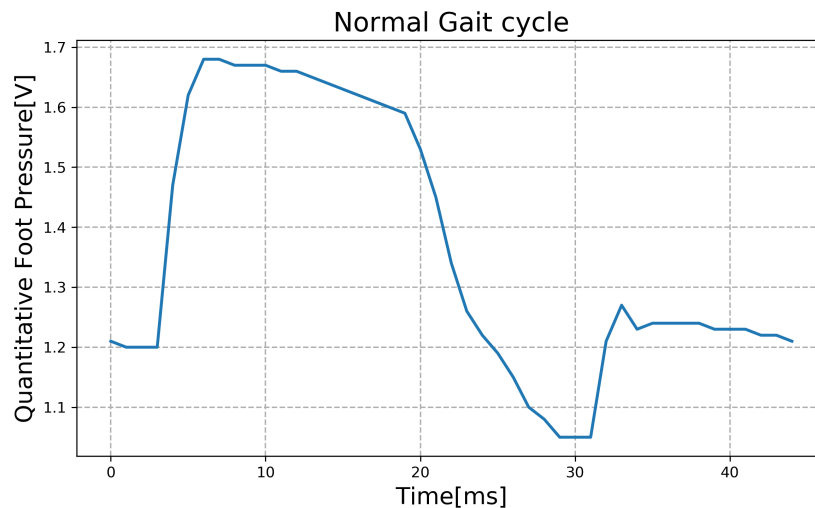
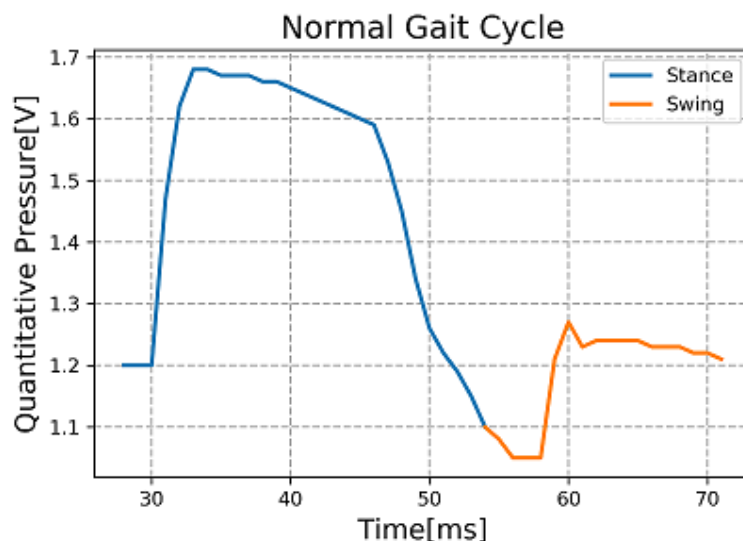


Figure 4.8: Confusion matrix; on classification of stance and swing phases



(a) Unclassified gait cycle input to DNN



(b) DNN classified output into Stance and Swing phases

Figure 4.9: Gait phase classification using Deep neural network

## 4.4 Gait Parameter Estimation

In this section, the classification results of the DNN model are used to calculate the gait parameters as discussed in section 2.1.6.

**Normalized peak pressure** values defines the ratio of peak values of plantar pressure regions subjective to body weight visualized in Figure 4.10

The temporal information obtained through classification of gait cycle into Stance and Swing phases is used to calculate **Stance ratio** as shown in Figure 4.11.

The temporal duration between two adjacent stance phases gives us **Step time** as shown in Figure 4.12

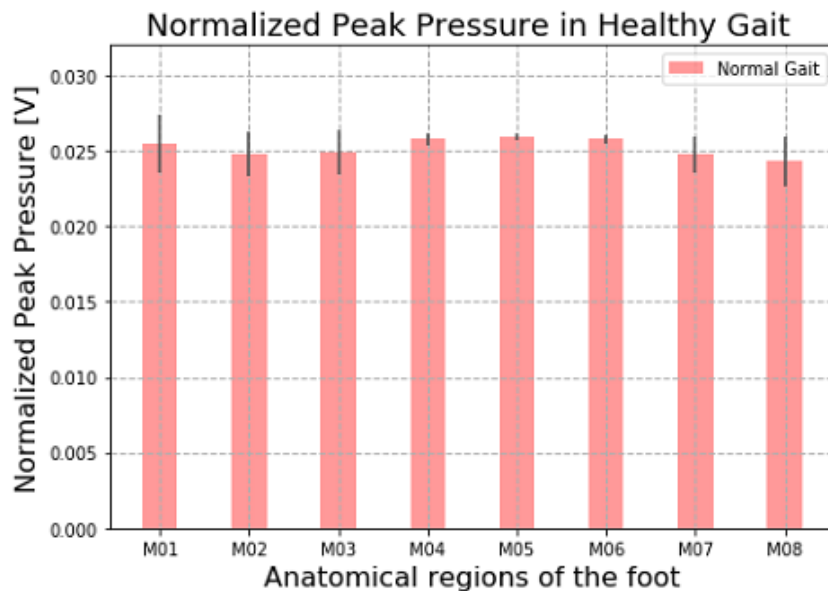


Figure 4.10: Normalized peak pressure values calculated on the dataset acquired from the experiments; a symmetrical distribution of the plantar pressure can be seen in all anatomical regions

## 4.5 Summary

A Machine learning framework for gait analysis was developed. A Deep neural network (DNN) was proposed for classification of gait phases, stance and swing. To avoid the brute force approach we used genetic algorithm to find the optimal hyper-parameters which reduced 80% of the parameter tuning time. The model achieved a 98% of inter-class classification accuracy depicted in Figure 4.9.

The output of the DNN was used to compute gait parameters that characterize human

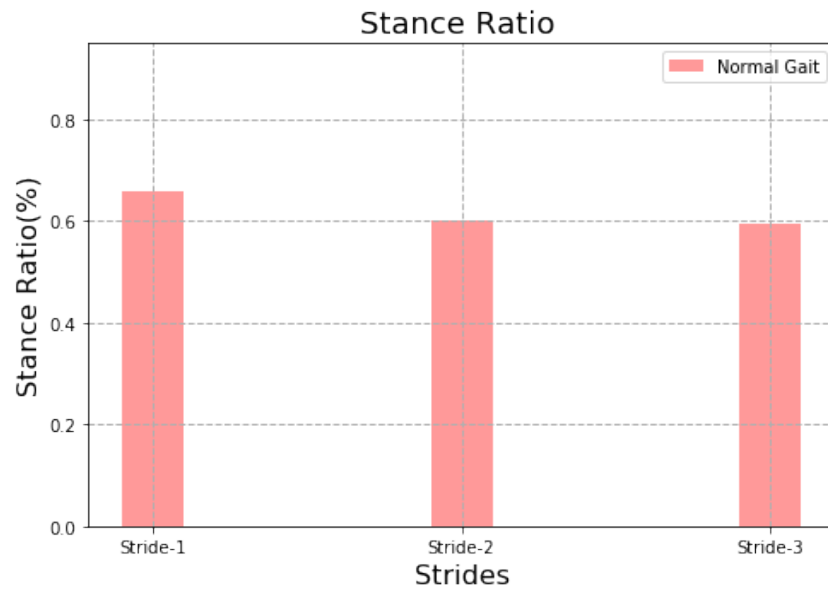


Figure 4.11: Stance Ratio (60%); in accordance with definitions of RLA terminology [1]

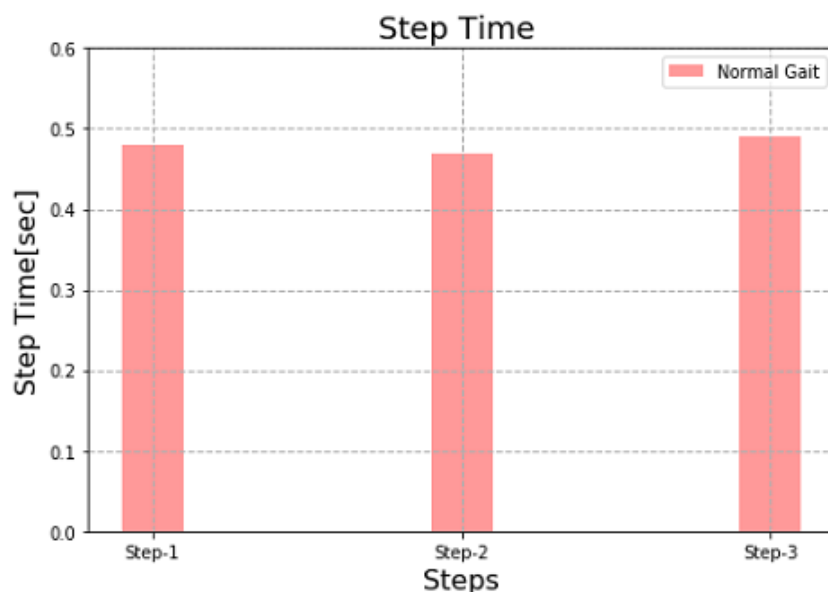


Figure 4.12: Step time

gait. Normal gait generally constitutes 60% of Stance time and 40% of Swing time. The proposed DNN was able to learn and classify the temporal patterns close to an accuracy of 98% . Symmetrical distribution of the weight / pressure can be seen in the visualizations of the gait parameters shown in Figures 4.10, 4.11 and 4.12. The classification results (60% - Stance time and 40% - Swing time ) and the symmetrical distribution of the gait parameters give us a clear intuition about the behavior of normal and healthy gait.

These characteristics of normal gait are used to identify the abnormal behaviors, a comparative analysis showcasing different metrics and gait parameters between normal and abnormal gait behaviors is depicted in the next chapter.

## **5 Abnormal Gait Analysis**

### **5.1 Introduction**

Abnormal gait is characterized as a behavior that deviates from normal gait due to different kinds of abnormalities / disorders. Abnormal gait is devoid of many significant gait functions like sensation, strength, coordination which are observed in a healthy(normal) gait. In-depth information on Etiology of gait abnormalities is presented in [36].

In this chapter, we present a novel methodology based on Machine learning to detect abnormal gait. The proposed methodology aims to demonstrate how advanced technologies help in gait diagnosis and treatment systems. At the end, three specific abnormalities associated with Spastic gait, Parkinsonian gait and Sensory-Ataxic gaits is presented.

### **5.2 Proposed Methodology**

In this section, we propose a methodology to detect abnormal gait by utilizing the characteristics of normal gait data analyzed and quantified in previous Chapter - 4, refer section 4.4. The experiments were conducted with 10 healthy individuals who were categorized into two different groups.

Natural gait data from first group containing 7 participants was collected, the procedure of the experiment was first explained to the participants and two inertial sensors are attached on the thigh and shank on both limbs, the pressure sensing insole was placed into respective foot wear and the PCB was fabricated into an enclosure shown in Figure 3.6. The participants were allowed to complete a natural walk of 10 meters as they would do in daily life shown in Figure 4.1.

Second group of participants were asked to simulate three specific gait abnormalities involving spastic gait, parkinson's gait and sensory ataxic gait as shown in Figures 3.6,3.7,3.8. Video references depicting such abnormalities were shown to the participants prior to their behavior simulation. The participants were allowed to complete a walk of 10 meters, each simulating the above mentioned gait abnormalities. Similar data

preprocessing techniques explained in Chapter - 4, section 4.3.1 were used to refine the raw sensor values.

### 5.3 Network Architecture

We train a stacked Long Short Term Memory Network (LSTM-model) using the dataset of the first group to predict the next subsequent sample in the time series. The data was reshaped to fit many to one architecture of the LSTM network, where the input sequence contained multi-dimensional sample features  $\mathbf{x} = [\mathbf{x}_1, \mathbf{x}_2, \dots, \mathbf{x}_N]$  in each step of an epoch. Here the parameter  $N$  is defined by the number of samples in one stride time. Figure 5.1 shows the high-level architecture of the LSTM model. The prediction model learns to predict  $l$  values; here  $l=1$  for  $N$  of the input variables. The training sequences (normal data) are divided into three sets: normal train ( $t_n$ ), normal validate ( $n_v$ ) and normal test ( $n_t$ ). The abnormal data is also segmented into abnormal validate ( $a_v$ ) and abnormal test ( $a_t$ ).

For training, we use the Mean-Squared-Error loss function. Given the ground truths,  $\mathbf{y} = [y_1, y_2, \dots, y_N]$  and the predicted output vector by the LSTM model,  $\hat{\mathbf{y}} = [\hat{y}_1, \hat{y}_2, \dots, \hat{y}_N]$  the mean-squared error loss function is calculated as

$$loss(\mathbf{y}, \hat{\mathbf{y}}) = \frac{1}{N} \sum_{n=1}^N (y_n - \hat{y}_n)^2 \quad (5.1)$$

#### 5.3.1 Long - Short Term Memory Networks

LSTM's are Recurrent Neural Networks(RNNs), which are capable of learning complex patterns especially long and short term dependencies in data. The internal state of an LSTM is responsible for specific functions such as forget, remember and update shown in Figure 5.2. The input-output relations [2] for one time step in a cell  $t$  are:

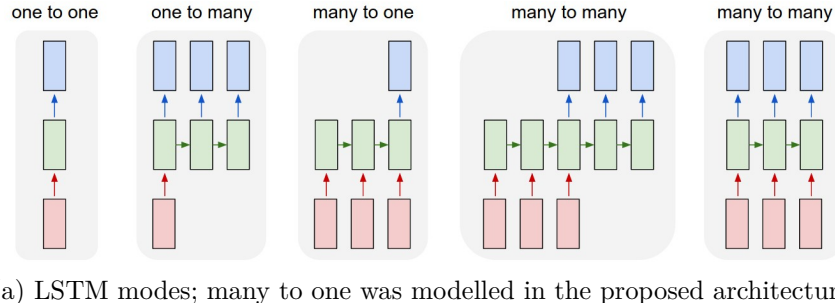
$$f_t = \sigma(W_f[h_{t-1}, x_t] + b_f) \quad (5.2)$$

$$r_t = \sigma(W_r[h_{t-1}, x_t] + b_r) \quad (5.3)$$

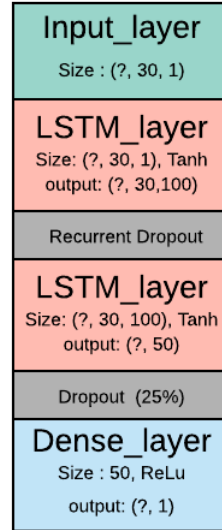
$$C_t = \tanh(W_u[h_{t-1}, x_t] + b_u) \quad (5.4)$$

$$C_t = f_t * C_{t-1} + r_t C_t \quad (5.5)$$

$$o_t = \sigma(W_o[h_{t-1}, x_t] + b_o) \quad (5.6)$$



(a) LSTM modes; many to one was modelled in the proposed architecture



(b) Proposed stacked LSTM

Figure 5.1: High-level architecture of the proposed stacked LSTM Network, here  $N = 30$ ,  $l = 1$  is shown as an example which depicts many to one network model [2]

$$h_t = o_t * \tanh(C_t) \quad (5.7)$$

where  $x_t \in R^n$  is the vector representing discrete input at time  $t$  and  $\sigma(\cdot)$  sigmoid activation function. In this,  $*$  denotes element wise product.  $h_t$  and  $h_{t-1}$  are the outputs of hidden layers at respective time instances.  $f_t, o_t, r_t$  are the cell  $C_t$  states  $f_t$  representing forget gate which manipulates the addition of activation to the output,  $o_t$  controls the internal state on the next cell.  $r_t * C_t$  functions for remembering and updating  $x_t$ . A standard LSTM contains a total of  $4(l + n) + 4l$  parameters that are optimized during the training process.

Figure 5.3 shows the training progress of the proposed stacked LSTM model. Another variant known as Bi-directional LSTM network has twice as many parameters. In addition to stacked LSTM we also tried LSTM - Auto-encoder, seq-seq LSTM and Multilayer perceptron networks, but stacked LSTM network had better performance in learning the characteristics and also in robust predictions.

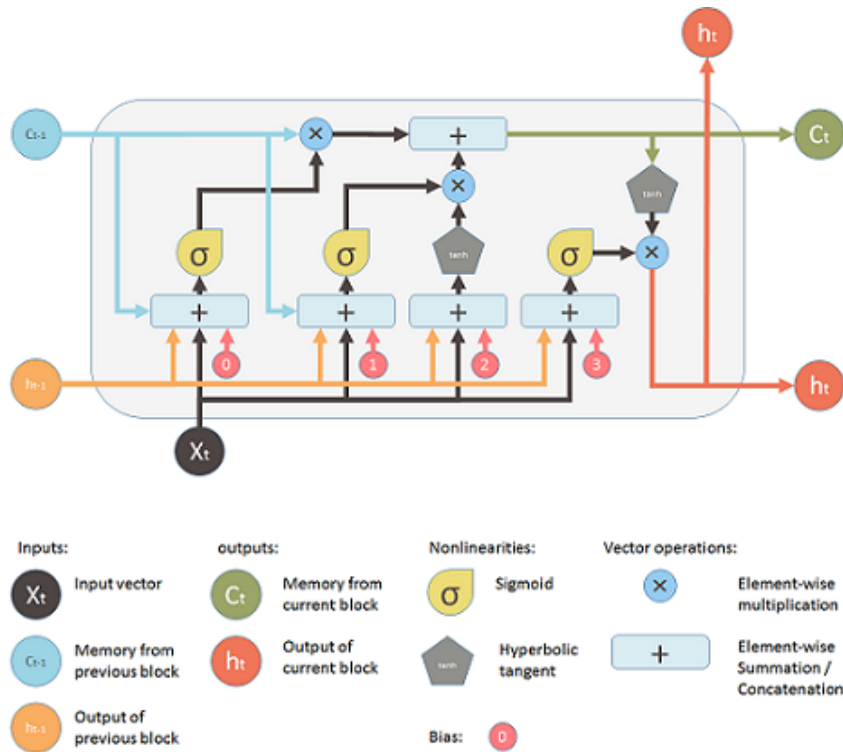


Figure 5.2: Components of a standard LSTM cell with weights, biases and activation functions. Input - Output relations are explained below in form of equations. The picture is partially borrowed from

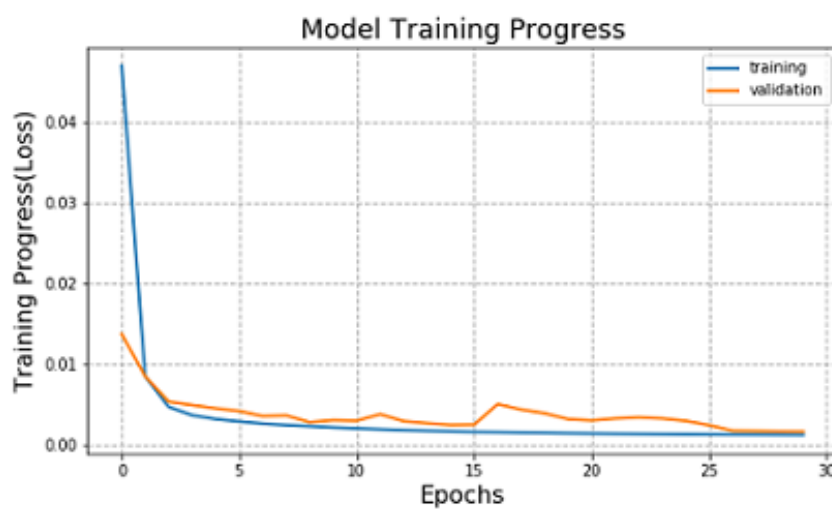


Figure 5.3: Training (blue) and Validation (orange) performance of our proposed stacked LSTM model on normal data

We use the prediction model and then calculate the error distribution using which we detect gait abnormalities. With a prediction length of  $l$ , each of the selected samples  $N$  in one stride we compute the prediction error vector for the input sequence  $x = [x_1, x_2, \dots, x_N]$  as  $e = [e_1, e_2, \dots, e_N]$  which is the difference between the respective ground truth and its predicted value at time  $t$ . The stacked LSTM model trained on  $t_n$  is used to compute the error vectors for each of sequences in the validation and test sets. This error vector is then used as a metric value for detecting abnormality. The LSTM prediction error against normal data is shown in Figure 5.4

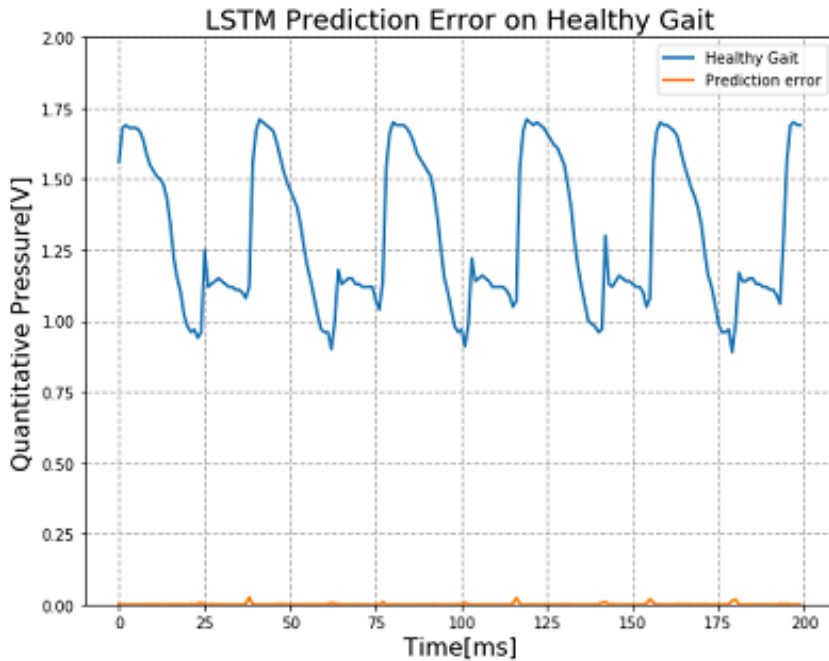


Figure 5.4: LSTM error predictions on healthy gait, shown in this plot are plantar pressure (blue) and predicted error (orange), depicts LSTM was accurate in predictions of normal gait behavior

## 5.4 Experiment and Results

### 5.4.1 Experiments

Three experiments were carried out by simulating abnormal gait behaviors over a 10 meters of walking path shown in Figure 4.1.

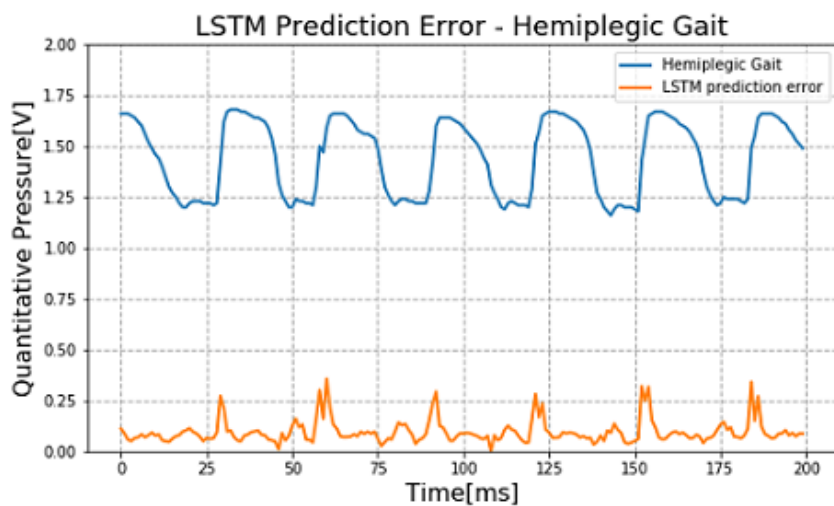
#### Spastic Gait

Spastic gaits are neurological gait disorders caused due to abrasion in the corticospinal tract [36]. The affected leg is often characterized by extension and plantar flexion;

circumduction of the leg is often seen during the swing phase and a flexed posture of the ipsilateral arm as shown in Figure 5.5



(a) Simulation of Spastic gait



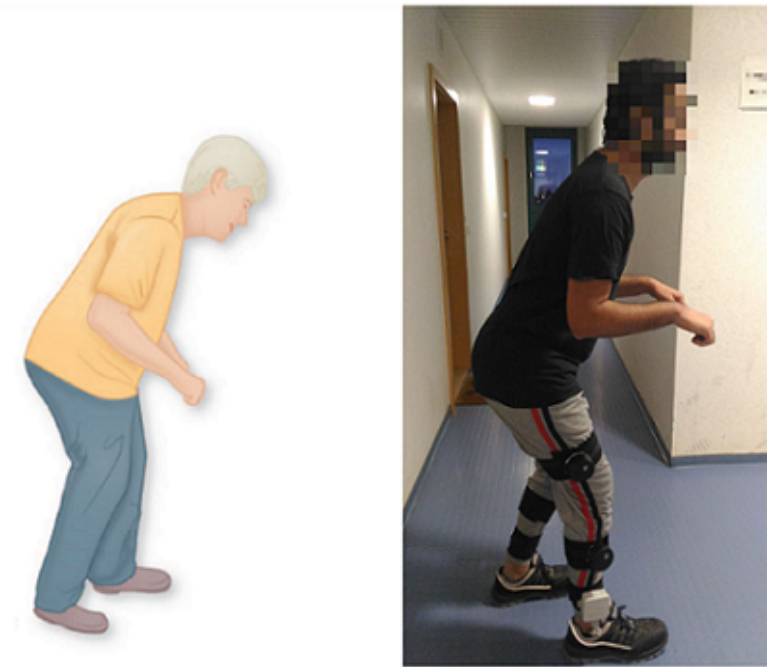
(b) LSTM prediction error against spastic gait

Figure 5.5: Characteristics of spastic gait [3] and Simulation of the same; LSTM prediction error

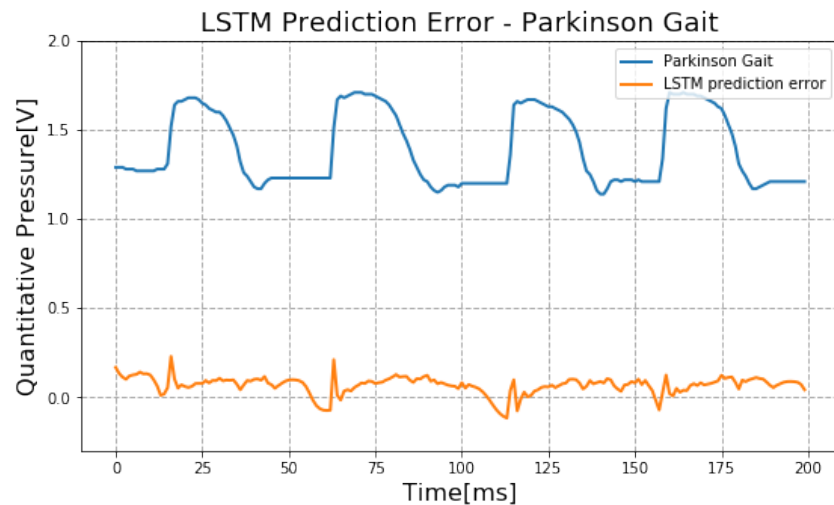
### Parkinsonian Gait

One of the most commonly gait disorder in elderly people is Parkinsonian gait. It is generally characterized by simultaneous rotation of trunk and pelvis [36]. In normal gait,

the rotation of trunk is followed by pelvis. Parkinson's disease is asymmetric in nature, arm swing and step length are affected and a tremor is also seen during walking.



(a) Simulation of Parkinsonian gait



(b) LSTM prediction error against parkinson gait

Figure 5.6: Characteristics of parkinson gait [3] and Simulation of the same; LSTM prediction error

### Sensory Ataxic Gait

This gait results in deficiency of the limb and joint position sense called as proprioception [36] resulting into a stomping situation as foot hits the ground as in Figure 5.7. Affected individuals are unable to feel the position of their foot relative to the ground, resulting in

an asymmetrical gait. Significant characteristics include shortened step length and wide based stance.

### 5.4.2 Results

The abnormalities have different levels of difficulty as far as detection is concerned. Error characteristics are also subjective and vary from each type of abnormality (see Figure 5.8). The error predictions against normal / healthy gait quantify to 2% whereas, the error predictions against the simulated abnormalities are in higher order of magnitudes quantifying between 20% to 25%. Therefore, we use this error vector as a detection metric of abnormality. Also, to validate the model output and to differentiate gait characteristics we calculate significant gait parameters that show contrasting difference between normal and abnormal behaviors.

We also report  $R^2$  regression function score, thereby evaluating the model predictions. It gives a measure of the likelihood of normal data to be predicted by the model. Best possible score is 1.0 and it can be negative (abnormal data).

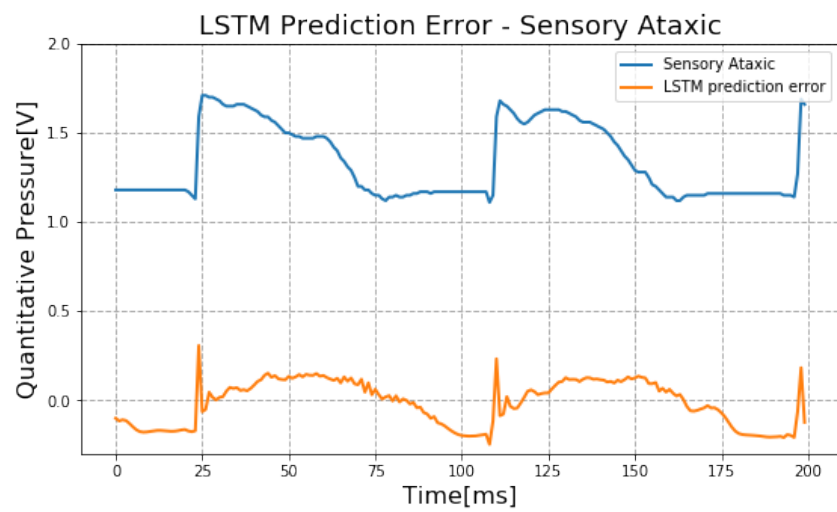
$$R^2(y, \hat{y}) = 1 - \frac{\sum_{i=0}^{n_{\text{samples}}-1} (y_i - \hat{y}_i)^2}{\sum_{i=0}^{n_{\text{samples}}-1} (y_i - \bar{y})^2} \quad (5.8)$$

## 5.5 Gait Parameter Estimation

A through literature review was carried out to present significant gait parameters that characterize human gait and show the clear difference between normal and abnormal behaviors. We present the following reliable parameters, the results of normalized peak pressure, stance ratio, step time, cadence, angles are expressed as the mean value with their standard deviations (SD) from multiple subjects and trials. The comparison between normal and simulated behaviors is expressed using the  $R^2$  metric. Table 5.1 shows the comparison of gait parameters results of the abnormal gaits and normal gait. Segment orientations such as thigh and shank are correlated using Pearson's Correlation Coefficient [63]. This correlation factor is also used to signify gait symmetry tabulated in Table 5.1. Figures 5.9, 5.10 show the statistical results (i.e., histograms and Box plots) of the gait parameters calculated in both the normal and abnormal walking experiments.



(a) Simulation of Sensory Ataxic gait



(b) LSTM prediction error against sensory ataxic gait

Figure 5.7: Characteristics of sensory ataxic gait [3] and Simulation of the same; LSTM prediction error

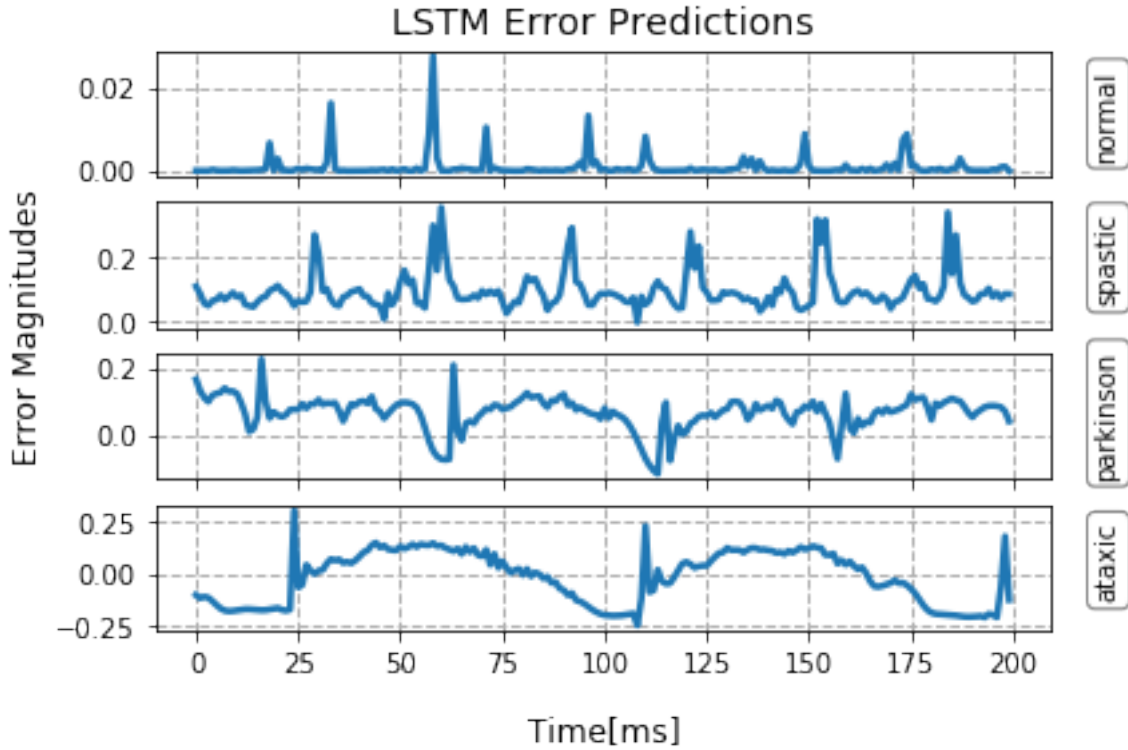


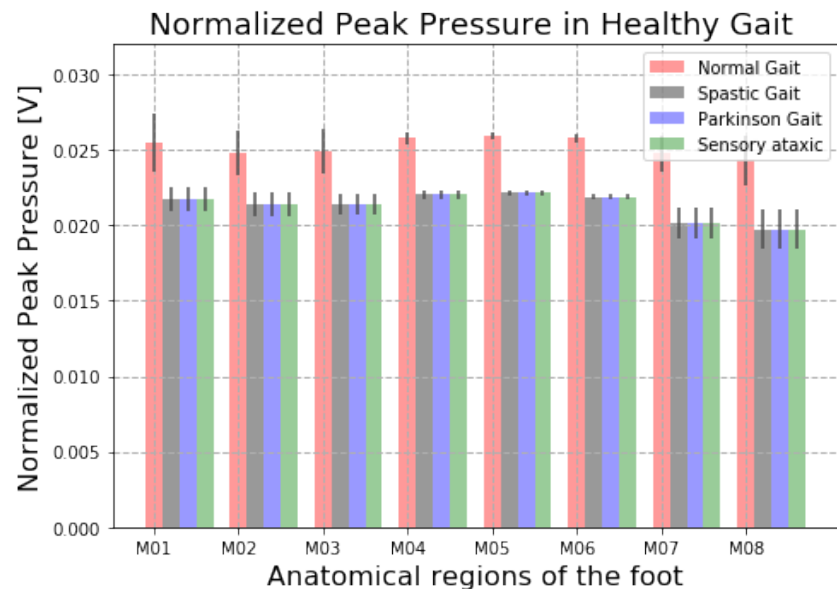
Figure 5.8: LSTM error predictions on simulated gait abnormalities, shown in this graphic are error plots from top to bottom: Normal, Spastic, Parkinson and Sensory-ataxic gaits. This predicted error is used as a detection metric of abnormality

Table 5.1: Comparison of gait parameters between Normal and Abnormal behaviors

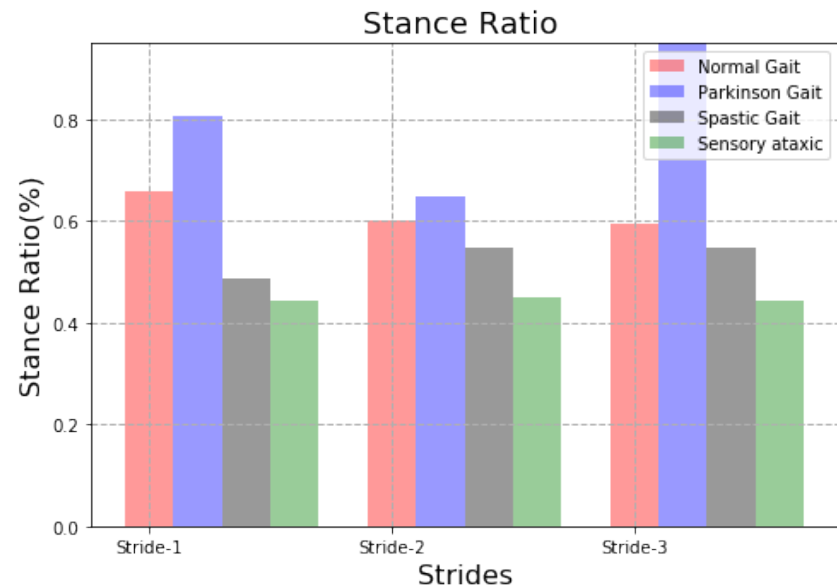
Parameters	Normal	Spastic	Parkinson	Ataxic
Stance-ratio (%)	$59.5 \pm 0.23$	$54.8 \pm 0.19$	$97.5 \pm 2.3$	$44.4 \pm 0.93$
Step-time(s)	$0.48 \pm 0.02$	$0.39 \pm 0.08$	$0.09 \pm 0.01$	$0.16 \pm 0.1$
Step-time variability(ms)	$6.679e-05$	6.2	0.15	0.28
Cadence (steps/min)	88	124	156	44
Angles	0.98	0.37	0.22	0.57
$R^2$	0.97	0.17	-0.29	-0.43
LSTM error(%)	2	$\pm 20$	$\pm 20$	$\pm 25$

## 5.6 Summary

The proposed stacked LSTM recurrent neural network demonstrates how abnormal gait behavior can be detected considering the characteristics of the error predictions see Figure 5.8 . Table 5.1 depicts a clear difference of gait parameters between normal and simulated abnormal gaits. Stance- ratio signifies unsymmetrical footing phases in parkinson (97.5%) and sensory ataxic (44.4%) gaits. Also, the shuffling appearance in parkinson gait and stomping behavior in sensory ataxic gaits results in decreased step length which in turn reduces the step time. A High deviation from normal cadence (88 steps/min) was observed



(a) Comparison plot of Normalized peak pressure between normal and abnormal gaits



(b) Stance ratio of normal and abnormal gaits

Figure 5.9: Comparison of Gait parameters; NPP and Stance Ratio

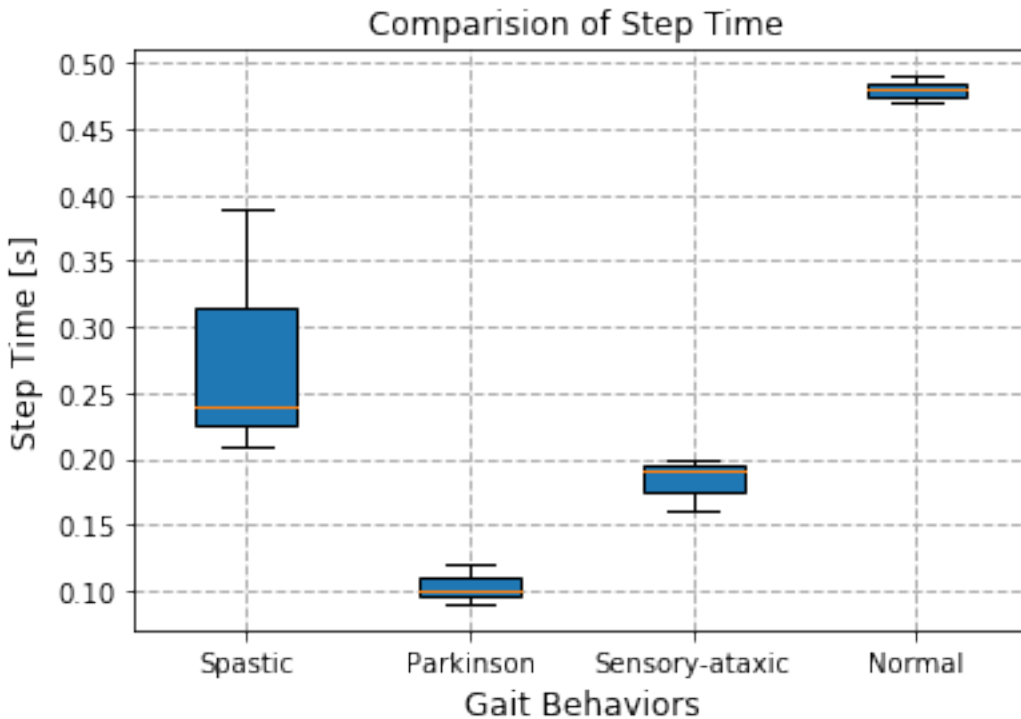


Figure 5.10: Comparison of Step time between normal gait and simulated abnormal gaits

in all abnormal gaits considering their specific characteristics. The unsymmetrical behavior of the simulated abnormal gaits was shown by the correlation factor calculated using Pearson's correlation coefficient [63]. The gait parameters and  $R^2$  metric shown in Table 5.1 show clear indication of the abnormality and also validate the output given by the LSTM model.

In conclusion, the proposed methodology depicts a feasible and reliable system to identify such abnormal behaviors. Future works include further investigation on calculating spatial parameters such as gait velocity, stride length that would be more beneficial for diagnosis and treatment systems. While the proposed work was carried through simulating abnormal behaviors, Further work is needed in the context of detecting abnormal behaviors in elderly people.

## **6 General Conclusions and Outlook**

This thesis work is aimed for developing a system that facilitates the use of wearable sensor technology integrated with state-of-the -art machine learning algorithms in biomedical systems, demonstrating how detection of functional disorders associated with human gait prior to their development helps in diagnosis and treatment systems. To what extent these objectives were determined is analyzed in the following chapter by assessing the main results of each chapter.

### **6.1 Conclusions on Proposed Frameworks**

In Chapter 3, a modular hardware setup for gait analysis was developed emphasizing the following goals and requirements explained in section 3.1. On the one hand, this includes design and development of plantar pressure measuring in-soles with piezo-resistive technology employing a matrix structure constituting 64 pressure sensing nodes. On the other hand, inertial sensor system (sensors and algorithms -Kalman filtering) were proposed for measurement of segment orientations from two inertial sensors of which one is mounted on thigh and other on shank segments. A wireless mobile based data acquisition system was designed in java script to visually guide the individual throughout the experiment. The insole was segmented into eight different anatomical regions displayed in Figure 3.9 which helped us in a detailed investigation of the pressure distributions. A 3D visualization of the in-sole depicting the quantitative pressure in Figure 3.10 gives a clear intuition about the weight shift during gait phases. Unlike vast majority of previous approaches, the proposed methodology uses significant plantar regions, thigh and shank orientations for analyzing human gait. Therefore, the developed hardware and data acquisition systems pave the way for a plug-and-play gait analysis in any terrain. To this end gait data acquisition in the wild was also successfully tested.

While, the gait phase classification was demonstrated in Chapter 4, the potential of machine learning algorithms especially artificial neural networks is depicted. Preprocessing techniques such as data normalization, butter-worth filtering and data augmentation were briefly discussed. Experiments involving a group of individuals were executed in an open environment as displayed in Figure 4.1. The proposed Deep neural network with the

following parameters in Figure 4.5 was trained using cross entropy loss function to classify gait phases; stance and swing. The effectiveness of using evolution algorithms such as genetic algorithm was determined by reducing the parameter tuning time to 80% which gave us an advantage in faster training process of the neural network. The gait phase classification accuracy achieved by the model was 98% and all findings such as model output, gait parameters are displayed in Figures 4.9, 4.10, 4.11, 4.12.

Likewise, in Chapter 5, we proposed a novel methodology by exploiting the characteristics of normal gait quantified in Chapter 4 to identify abnormal gait behaviors. Experiments simulating three specific abnormal behaviors related to spastic gait (Figure 5.5), parkinson gait (Figure 5.6) and sensory ataxic gait (Figure 5.7) were carried out. The framework includes a stacked LSTM recurrent neural network shown in Figure 5.1, which was trained to learn the temporal patterns of normal gait. The prediction error was then used as a metric to identify gait abnormality. The model prediction errors for the simulated abnormalities is displayed in Figure 5.8. We also compute relevant gait parameters that show contrasting difference between normal gait and abnormal gait through which we validate the output of the LSTM model. All the findings tabulated in Table 5.1 depict the potential of the proposed methodology to identify gait abnormalities.

## 6.2 Applications

The benefits of using wearable sensor system for gait analysis in biomedical applications were demonstrated by specific examples in the applications focused in Chapters 5 of this thesis. It was demonstrated that the performance of stacked LSTM model was definite through the error predictions. Recognition of specific functional gait disorders is one of the potential applications in the context of proposed methods.

Several biomedical applications in which measurement, classification tasks and identification of abnormal behaviors might be improved, from recognition to rehabilitation robotics and clinical assessment systems. Regardless of the specific application, the employment of the proposed methods will lead to less manual effort and parameter-adjustments and to more personalized health care solutions.

## 6.3 Future Research

Minor limitations of the work have already been mentioned in the starting sections of this thesis. In this section, these points are summarized and discussed in a broader sense.

Future work should be dedicated in determining the type of abnormality analyzing intra-subject predictions. Data from equivalent individuals should be acquired over a long period of time. On the sensory side, improving the form factor, design and embedding temperature sensors into the pressure sensing insoles might largely give more information for in-depth analysis. Also, effective and accurate computation of spatial parameters such as gait velocity, stride length can be achieved by retrieving spatial information from the employed sensors and also using regression based machine learning methods.

## Bibliography

- [1] Observational Gait. Analysis handbook; the professional staff association of rancho losamigos medical center: Downey, ca, usa. 1989.
- [2] Mahdi Hajiaghayi and Ehsan Vahedi. Code failure prediction and pattern extraction using LSTM networks. *CoRR*, abs/1812.05237, 2018.
- [3] ALLAN H. ROPPER. Adams and vctors principles of neurology. 2019.
- [4] J. Le E. Chalmers, D. Sukhdeep, J. Watt, J. Andersen, and E. Lou. Inertial sensing algorithms for long-term foot angle monitoring for assessment of idiopathic toewalking. *Gait Posture*, 39:1, 2014.
- [5] J. Goulermas A. Findlow, C. Nester, D. Howard, and L. Kenney. Predicting lower limb joint kinematics using wearable motion sensors. *Gait Posture*, 28:1, 2008.
- [6] A. Findlow J. Goulermas, C. Nester, P. Liatsis, X. j. Zeng, L. Kenney, P. Tresadern, S. Thies, and D. Howard. An instance-based algorithm with auxiliary similarity information for the estimation of gait kinematics from wearable sensors, ieee trans. *eural Netw.*, 19(9):15741582, 2008.
- [7] E. Spaich J. Rueterborries and O. Andersen. Gait event detection for use in fes rehabilitation by radial and tangential foot accelerations, med. *Eng. Phys*, 36:4, 2014.
- [8] B. Andrews R. Williamson. Gait event detection for fes using accelerometers and supervised machine learning, ieee trans. *Rehabil. Eng*, 8(3):312319, 2000.
- [9] E. Ambrosini N. Bejarano, A. Pedrocchi, G. Ferrigno, M. Monticone, and S. Ferrante. A novel adaptive, real-time algorithm to detect gait events from wearable sensors, ieee trans. *Neural Syst. Rehabil. Eng*, 23:3, 2015.
- [10] V. Genovese A. Mannini and A. Sabatini. Online decoding of hidden Markov models for gait event detection using foot-mounted gyroscopes, ieee j. In *Biomed. Health Inform.* 18 (4) 1122–1130, 2014.
- [11] S. Rossi J. Taborri, E. Palermo, F. Patanè, and P. Cappa. A novel hmm distributed classifier for the detection of gait phases by means of a wearable inertial sensor

- network. *Sensors*, 14:9, 2016.
- [12] A. López R. González and J. Rodriguez-Uría. D. Álvarez, j. Alvarez, *Real-time gait event detection for normal subjects from lower trunk accelerations*, *Gait Posture*, 31:3, 2010.
- [13] S. Thies M. Aung, L. Kenney, D. Howard, R. Selles, A. Findlow, and J. Goulermas. Automated detection of instantaneous gait events using time frequency analysis and manifold embedding, *ieee trans. Neural Syst. Rehabil. Eng.*, 21:6, 2013.
- [14] A. Sabatini A. Mannini. Gait phase detection and discrimination between walking jogging activities using hidden Markov models applied to foot motion data from agyroscope. *Gait Posture*, 36:4, 2012.
- [15] M. Gavrilovic N. Mijailovic and S. Rafajlovic. Gait phases recognition from accelerationsand ground reaction forces: application of neural networks. *Telfor J.*, 1:1, 2009.
- [16] S. Sua M. Yuwono, Y. Guob, B. Moultona, and H. Nguyenna. Unsupervised nonparametricmethod for gait analysis using awaist-worn inertial sensor, appl. *Soft Comput.*, 14, 2014.
- [17] A. Yang E. Guenterberg, H. Ghasemzadeh, R. Jafari, R. Bajcsy, and S. Sastry. A methodfor extracting temporal parameters based on hidden Markov models in body sensornetworks with inertial sensors, *ieee trans. inf.* In *Technol. Biomed.* 13 (6) 1019–1030, 2009.
- [18] D. Lai B. Santhiranayagam, W. Sparrowa, and R. Begg. A machine learning approach to estimate minimum toe clearance using inertial measurement units, j. *Biomech.*, 48:16, 2015.
- [19] X. Xu B. Dobkin, M. Batalin, S. Thomas, and W. Kaiser. Reliability and validity of bilateral ankle accelerometer algorithms for activity recognition and walking speed after stroke. *Stroke*, 42:8, 2011.
- [20] C. Angulo A. Samà, D. Pardo, A. Català, and J. Cabestany. Analyzing human gait and posture by combining feature selection and kernel methods. *Neurocomputing*, 74:16, 2011.
- [21] A. Muñoz-Meléndez I. López-Nava, A. P. Sanpablo, A. A. Montero, I. Q. Urióstegui, and L. N. Carrera. Estimation of temporal gait parameters using Bayesian models on acceleration signals, *comput.* In *Methods Biomech. Biomed. Eng.* 19 (4) 396–403,

2016.

- [22] A. Sabatini A. Mannini. Walking speed estimation using foot-mounted inertial sensors: comparing machine learning and strap-down integration methods, med. *Eng. Phys.*, 36:10, 2014.
- [23] D. Trojaniello A. Mannini, A. Cereatti, and A. Sabatini. A machine learning framework for gait classification using inertial sensors: application to elderly. *post-stroke and huntingtons disease patients, Sensors*, 16:1, 2016.
- [24] T. Lockhart J. Zhang and R. Soangra. Classifying lower extremity muscle fatigue during walking using machine learning and inertial sensors, annu. In *Biomed. Eng.* 42 (3) 600–612, 2015.
- [25] Abdul Hadi Abdul Razak, Aladin Zayegh, Rezaul K. Begg, and Yufridin Wahab. Foot plantar pressure measurement system: A review. In *Sensors*, 2012.
- [26] Cunguang Lou, Shuo Wang, Tie Liang, Chenyao Pang, Lei Huang, Mingtao Run, and Xiuling Liu. A graphene-based flexible pressure sensor with applications to plantar pressure measurement and gait analysis. *Materials*, 10(9):1068, sep 2017.
- [27] Mihaela Baritz and Diana Cotoros. Analysis of plantar pressures developed during gait for hollow foot and flat foot shapes with bio-behavioral implications. *2011 E-Health and Bioengineering Conference, EHB 2011*, 01 2011.
- [28] J. Zhang and R. Soangra T. Lockhart. Classifying lower extremity muscle fatigue during walking using machine learning and inertial sensors, annu. In *Biomed. Eng.* 42 (3) 600–612, 2015.
- [29] M. Yang, H. Zheng, H. Wang, S. McClean, J. Hall, and N. Harris. A machine learning approach to assessing gait patterns for complex regional pain syndrome, med. *Eng.Phys.*, 34:6, 2012.
- [30] T. Kautz J. Hannink. *Sensor-based Gait Parameter Extraction with Deep Convolutional Neural Networks*. IEEE, EMBS.
- [31] Tanmay T. Verlekar. Luís d. oares, *Automatic Classification of Gait Impairments Using a markerless*, 18:9, Sep; 2018.
- [32] M. Hidalgo Francisco and Javier Ferrández-Pastor. A vision-based proposal for classification of normal and abnormal gait using rgb camera. *Journal of Biomedical Informatics*, 63:82–89, October 2016.

- [33] C. Vaughan, B. Davis, and J. O'Connor. *Dynamics of human gait*. Kiboho Publishers, Cape Town, South Africa, 1999.
- [34] J. Perry and J. M. Burnfield. *Gait Analysis: Normal and Pathological Function*. Slack Inc, New York, NY, 2010.
- [35] P. Mahlknecht, S. Kiechl, B. R. Bloem, et al. Prevalence and burden of gait disorders in elderly men and women aged 60–97 years: a populationbased study. *PLoS ONE*, 8:7, 2013.
- [36] Jessica M. Baker. Gait disorders. *The American Journal of Medicine*, 131(6):602–607.
- [37] A. Aboutorabi, M. Arazpour, M. Bahramizadeh, S. W. Hutchins, and R. Fadayevatan. The effect of aging on gait parameters in able-bodied older subjects: a literature review. *Aging Clin Exp Res*, 28(3):393–405, 2016.
- [38] A. H. Ropper, M. A. Samuels, and 7. Klein Jp. Chapter. Disorders of stance and gait. In M. A. Samuels and J. P. Klein, editors, *Ropper AH*, pages 115–126. McGaw-Hill;, Principles of Neurology. 10th ed. New York, NY, 2017.
- [39] M. Hong, J. S. Perlmutter, and Earhart Gm. A kinematic and. and electromyographic analysis of turning in people with parkinson disease. *Neurorehabil NeuralRepair*, 23(2):166–176, 2009.
- [40] K. Smulders, M. L. Dale, P. Carlson-Kuhta, J. G. Nutt, and Horak Fb. Pharmacological treatment in parkinsons disease: effects on gait. *Parkinsonism Relat Disord*, 31:3–13, 2016.
- [41] N. Giladi and Nieuwboer A. Understanding and. and treating freezing of gait in parkinsonism, proposed working definition, and setting the stage. *Mov Disord*, 23:S423–S425, 2008.
- [42] J. G. Nutt, B. R. Bloem, N. Giladi, M. Hallett, F. B. Horak, and Nieuwboer A. Freezing of gait:. moving forward on a mysterious clinical phenomenon. *ancet Neurol*, 10(8):734–744, 2011.
- [43] G. K. Kerr, C. J. Worringham, M. H. Cole, P. F. Lacherez, J. M. Wood, and Silburn Pa. Predictors of future falls in parkinson disease. *Neurology*, 75(2):116–24, 2010.
- [44] G. Ebersbach, C. Moreau, F. Gandor, L. Defebvre, and Devos D. Clinical syndromes:Parkinsonian gait. *Mov Disord*, 28(11):1552–1559, 2013.
- [45] J. M. Baker and Sudarsky L. Gait disorders. balance and falls. In A. S. Fauci, D. L.

- Kasper, S. L. Hauser, D. L. Longo, and J. Loscalzo, editors, *Jameson JL*, pages 1–20. McGraw-Hill, New York, 2018.
- [46] J. G. Nutt, C. D. Marsden, and Thompson Pd. Human walking and. and higher-level gait disorders, particularly in the elderly. *Neurology*, 43(2):268–279, 1993.
- [47] Dr.Thomas Seel. Learning control and inertial realtime gait analysis in biomedical applications. Phd. dissertation, Technischen Universität Berlin, 2015.
- [48] O. J. Woodman. an introduction to inertial navigation. Technical Report 696, University of Cambridge, 2007.
- [49] A. D. Young. *Comparison of orientation filter algorithms for realtime wireless inertial posture tracking*. In Wearable and Implantable Body Sensor Networks, 2009. BSN 2009. Sixth International Workshop on, pages 5964, 2009.
- [50] Dan Simon. Kalman filtering. *Embedded Systems Programming*, 14:6, 2001.
- [51] Kyoungchul Kong and M. Tomizuka. A gait monitoring system based on air pressure sensors embedded in a shoe. *IEEE/ASME Transactions on Mechatronics*, 14(3):358–370, 2009.
- [52] Hui Yu et al. A walking monitoring shoe system for simultaneous plantar-force measurement and gait-phase detection. In *2010 IEEE/ASME International Conference on Advanced Intelligent Mechatronics*, 2010.
- [53] I. Gonzlez, J. Fontecha, R. Hervs, and J. Bravo. An ambulatory system for gait monitoring based on wireless sensorized insoles. *Sensors*, 15:16589–16613, 2015.
- [54] B. A. MacWilliams and P. F. Armstrong. Clinical applications of plantar pressure measurement in pediatric orthopedics. In *Proceeding of Pediatric Gait, 2000. A New Millennium in Clinical Care and Motion Analysis Technology*, , IL, USA, 22 pp. 143150. 2000.
- [55] E. Zheng, B. Chen, K. Wei, and Q. Wang. Lower limb wearable capacitive sensing and its applications to recognizing human gaits. *Sensors*, 13:13334–13355, 2013.
- [56] Aoife Healy et al. Repeatability of walkinsense in shoe pressure measurement system: A preliminary study. *The Foot*, 22(1):35–39, 2012.
- [57] Ranveer Joyseeree, Rami Abou Sabha, and Henning Müller. Applying machine learning to gait analysis data for disease identification. *Studies in health technology and informatics*, 210:850–4, 05 2015.

- [58] G. Li, T. Liu, T. Li, Y. Inoue, and J. Yi. Neural network-based gait assessment using measurements of a wearable sensor system. In *2014 IEEE International Conference on Robotics and Biomimetics (ROBIO 2014)*, pages 1673–1678, Dec 2014.
- [59] S. M. N. A. Senanayake, J. Triloka, O. A. Malik, and M. Iskandar. Artificial neural network based gait patterns identification using neuromuscular signals and soft tissue deformation analysis of lower limbs muscles. In *2014 International Joint Conference on Neural Networks (IJCNN)*, pages 3503–3510, July 2014.
- [60] Y. Sun, G. Yang, and B. Lo. An artificial neural network framework for lower limb motion signal estimation with foot-mounted inertial sensors. In *2018 IEEE 15th International Conference on Wearable and Implantable Body Sensor Networks (BSN)*, pages 132–135, March 2018.
- [61] Abien Fred Agarap. Deep learning using rectified linear units (relu). *CoRR*, abs/1803.08375, 2018.
- [62] Felipe Petroski Such, Vashisht Madhavan, Edoardo Conti, Joel Lehman, Kenneth O. Stanley, and Jeff Clune. Deep neuro evolution: Genetic algorithms are a competitive alternative for training deep neural networks for reinforcement learning. *CoRR*, abs/1712.06567, 2017.
- [63] Chester Rei E. Duhaylungsod, Czarina Eloise B. Magbitang, Jan Faith Isaac R. Mercado, George Elison D. Osido, Shannen Andrea C. Pecho, and Angelo R. Dela Cruz. Detection of gait abnormality through leg symmetry and temporal parameters. *2017 IEEE 9th International Conference on Humanoid, Nanotechnology, Information Technology, Communication and Control, Environment and Management (HNICEM)*, 2017.